GRS

Modelling Gas and
Water Flow through
Dilating Pathways
in Opalinus Clay

The HG-C and HG-D
Experiments

GRS

Modelling Gas and Water Flow through Dilating Pathways in Opalinus Clay

The HG-C and HG-D Experiments

A Study within the Euratom
7th Framework Programme
Project FORGE

Martin Navarro

March 2013

Remarks

The present study was undertaken within the framework of the EC project FORGE in the 7th framework programme. The FORGE project is a pan-European project with links to international radioactive waste management organisations, regulators and academia, specifically designed to tackle the key research issues associated with the generation and movement of repository gases.

Contents

1   Introduction

In several countries, clay stone is considered to be a possible host rock for the disposal of radioactive waste. Due to the low permeability of clay stone the generation and migration of gases inside the repository system is an issue that has to be considered in performance assessments. In the repository, gas is mainly generated by metal corrosion and degradation of organic matter, which may be part of low- or intermediate-level waste. The pressure build-up caused by gas generation changes the hydraulic state of the repository and may lead to contaminant transport or barrier violation. A good understanding of gas migration is needed to assess the impacts of gas generation and to allow safety statements with sufficient confidence.

Shortly after repository closure, the most permeable path for gas migration is given by the excavation-damaged zone (EDZ). This pathway can be interrupted by the local removal of disturbed rock and subsequent emplacement of well-sealing technical barriers. Preferential pathways may also be given along the interfaces between engineered barriers and the host rock. If gas does not manage to escape along these ways, it is forced to enter the host rock formation.

Gas transport in the host rock becomes more efficient as gas pressure rises. This increase of efficiency is not a gradual process but one that is controlled by pressure thresholds, which mark the onsets of new transport mechanisms. As pressure builds up, the simple diffusion process is first accompanied by visco-capillary flow and afterwards by the opening of microscopic pathways [1], a process often referred to as "pathway dilation". At even higher pressures, macroscopic fracturing may occur. If pathway dilation or fracturing takes place, a vertical escape of gas through the host rock is fostered by the upward-decrease of the lithostatic pressure [2]. However, heterogeneities or anisotropies of the rock like bedding planes may favour other directions of gas migration.

Which mechanisms of gas migration will come into effect during the evolution of a repository can be influenced by means of repository design or waste conditioning. Providing room for gas storage or reducing gas generation, for instance, may regulate the velocity and amplitude of the pressure rise and prevent the occurrence of pathway dilation or fracturing. Thus, the probability and relevance of each gas transport process

depends on the chosen repository concept and layout and cannot be determined in general.

In order to study the process of gas migration in Opalinus Clay, Nagra has conducted several long-term in-situ tests at the Mont Terri Rock Laboratory, Switzerland. Since 1999, four experiments have been carried out at the same site: The GP-A, GS, HG-C, and HG-D experiments, which used an array of four to five boreholes for fluid injection and monitoring.

In the GP-A experiment, a hydraulic fracture has been created. This fracture was tested in the following GS experiment [3]. From 2006 to 2009, after a period of possible self-sealing, the fracture was re-tested in the HG-C experiment [4, 5]. In order to investigate the behaviour of the undisturbed clay, a new borehole has been drilled within the framework of the HG-D experiment, approximately 1 metre below the expected location of the GP-A fracture. From 2009 to 2012, liquid and gas injection tests were performed using the new borehole. Both the HG-C and the HG-D experiment have been carried out in two phases. Phase 1 was a long-term water injection test and phase 2 a long-term gas injection test.

In the FORGE project, GRS contributed to the analysis and interpretation of the HG-C and HG-D experiments by numerical modelling. The main questions of this study were:

- Which models are able to reproduce the experimental observations?

- Do these models improve the understanding of gas flow in the clay host rock?

It is well known that the two-phase flow theory is not able to capture many important aspects of gas flow in clay [6, 7]. Still, two-phase flow codes and modified versions are frequently used in the field of performance assessment for deep geological repositories [8-12]. Modellers apparently still find that the two-phase flow theory is a good description of many gas transport situations in clay and a good starting point for the derivation of more sophisticated models. Thus it is likely that two-phase flow models will remain in use in performance assessments for some time. The capabilities and limitations of two-phase flow models should therefore be investigated thoroughly and in a differentiated way. This was also attempted in this study.

In the present work, two categories of models were used. The first category was based on the two-phase flow code TOUGH2/EOS7, which has been written by the Lawrence

Berkeley National Laboratory, Berkeley, USA [13-15]. The second category comprises simple models for gas flow, which are referred to as "tube-chamber models" in the following. These models describe the flow of gas inside a tube, which is the connecting element between the injection borehole and an air-filled chamber. Different properties can be attributed to the porous medium inside the tube.

The applied models appear to be simple in consideration of the fact that pathway dilation results from the close interaction of hydraulic and mechanical processes. Although the mentioned codes are not hydro-mechanical codes, they consider the effects of hydro-mechanical processes in a simplified way. The advantage of simplifying modelling approaches is that they bring out the main aspects of the system and avoid the generation of models with a lot of parameters whose individual relevance is difficult to see. Simplified models are far easier to understand in terms of cause and effect. On the basis of this understanding it will be easier to compose adequate conceptual and physical models in the future.

The water and gas injection phases of the HG-C experiment and the gas injection phase of the HG-D experiment were investigated in chronological order. The original version of TOUGH2 was used first. From this starting point, model improvements were successively developed.

Chapter 3 examines the water injection phase of HG-C by means of the original TOUGH2 code and a variable permeability model. The analysis of the gas injection phase of HG-C, which uses a pathway dilation and a tube-chamber model, is described in chapter 4. Chapter 5 investigates the gas injection phase of HG-D by means of another tube-chamber model. The results are discussed in chapter 6 taking into account the results of the GP-A and GS experiments, which have been performed previously at the same site. General conclusions are drawn in chapter 7.

2   Site description

At the experimental site, four boreholes (BGS1, BGS2, BGS3, and BGS4) of approx. 12 m length have been drilled into the Opalinus Clay formation (shaly facies) perpendicular to the bedding planes with a dip of approx. 50°. These boreholes were used for the GP-A, GS, HG-C, and HG-D experiments by Solexperts [4, 5, 16]. Boreholes BGS1 and BGS2 were equipped with triple packer systems, boreholes BGS3 and BGS4 with "Fixed Re-Installable Micrometres" (FIMs) in order to observe the deformation of the Opalinus Clay (see Fig. 2.1). The bottom interval of each borehole was labelled "interval 1", the central interval "interval 2" and the top interval "interval 3". The central interval of BGS2 was used for the injection of water and gas in the GP-A, GS, and HG-C experiments.

In June 2009, an additional borehole (BHG-D1) was drilled at the HG-C site. It was equipped with a triple packer system in November 2009 [16]. The central interval of BHG-D1 is located approximately 1 m below the expected location of the fracture which has been created in the GS-experiment (see Fig. 2.2). The equipment of the boreholes BGS1, BGS2, BGS3, and BGS4 remained the same as in the HG-C experiment.

The HG-D experiment has been carried out in two phases. Phase 1 was a multistep water injection test which was performed in interval 2 of borehole HGD from 29th April 2010 until 16th August 2010 (shut-in). Phase 2, a multistep gas injection test, followed from 29th December 2010 to 23rd February 2012. The experimental set-up was similar to that of the HG-C experiment. In the present study, only the gas injection phase of the HG-D experiment was investigated.

Within the framework of the FORGE project, Nagra has provided field data and internal reports for the GP-A, GS, HG-C and HG-D experiments.
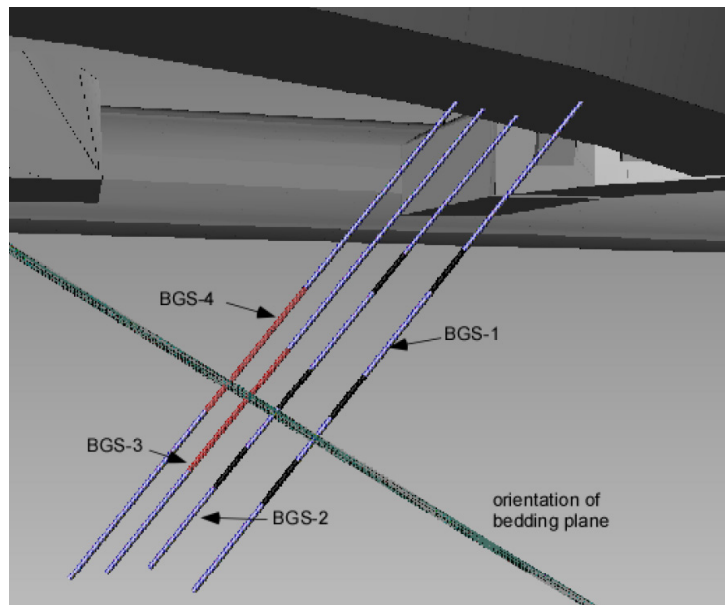
Fig. 2.1 3D view of the HG-C boreholes showing the orientation of the bedding planes (taken from [5])
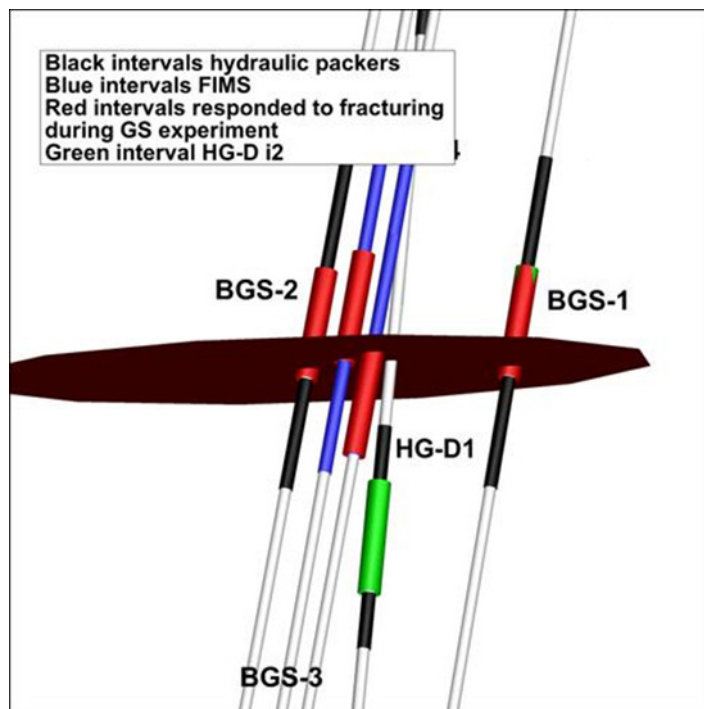
Fig. 2.2 Schematic figure showing the relative location of borehole intervals in the HG-D experiment and the assumed shape and location of the fracture that has been created in the GP-A experiment (Figure used with kind permission of Nagra)

3 HG-C Phase 1 (water injection)

3.1 Experimental results and data evaluation

Fig. 3.1 shows the experimental devices for the pressurisation of interval 2 of BGS2 (the packer system inside BGS2 and the monitoring boreholes are not displayed). The injection pressure was controlled by pressure vessel number 3. At the beginning of each pressure step, the vessel was pressurised with gas. Then, during the pressure step, the gas reservoir inside the vessel was shut in. Changes of injection pressure during a pressure step relate to the outflow of water from the pressure vessel and the expansion of the gas reservoir inside the vessel.

The following raw data has been provided for phase 1 of the HG-C experiment:

- Pressures in all packer intervals in kPa

- FIM measurements in BGS3 and BGS4 in mm/m

- Flow rates in ml/min. (time series "Qhigh" and "Qlow"; according to instructions from Nagra, the Qlow data should be used)

- Pressure in pressure vessel 3 in kPa

- Air temperature in °C

- Weight of pressure vessel 3 in g

Interval 2 of borehole BGS2 will be referred to as "injection interval" in the following. Consequently, the pressure measured in the injection interval and the flow into this interval will be referred to as "injection pressure" and "injection flow", respectively.

Six pressure steps with increasing pressure (named "1+", "2+", "3+", "4+", "5+", and "6+") and five pressure steps with decreasing pressure (named "5-", "4-", "3-", "2-", and "1-") have been performed. The results of the pressure, flow, and deformation measurements are displayed in Fig. 3.2 and Fig. 3.3.

No problems have been reported regarding the FIM measurements. For the analysis of experimental phase 1, not all pressure measurements were used:

- Regarding borehole BGS2, only the pressure data of interval 2 for pressure step 2+ to 1- were used. The data for the other intervals were dismissed for the following reasons:

  – Interval 3 of BGS2 showed a quick response to the pressure rise in injection interval 2 (see Fig. 3.2). According to Trick [4] the fast response could point to compressibility effects of the packer rather than to a packer bypass. However, there seemed to be a leakage between interval 2 and 3 during pressure step 1+ (12 bar) because of the rapid pressure decrease in interval 2 (indicating water loss from interval 2) and the corresponding strong response in interval 3.

  – Trick [4] has assumed that interval 1 had a connection to the atmosphere. Thus, the pressure measurements for this interval were not considered in this study.

- Regarding borehole BGS1, only the pressure data of interval 3 were used. The data for the other intervals were dismissed for the following reasons:

  – During the redress of the packer system of borehole BGS1, a connection between interval 1 and the unsealed part of the packer mandrel has been detected [4].

  – Pressures of about 120 kPa (which are close to atmospheric pressure) have been measured in interval 2. This indicates that this interval was not at equilibrium with the pore water pressure.

From the data, it was possible to estimate the injection flows in three ways:

a) by using the flow meter measurements;

b) by using the injection pressure measurements; these reflect the expansion of the gas bubble inside pressure vessel 3 and thus are a measure of the water volume that was expelled from the vessel;

c) by using the measurements of the balance on which the pressure vessel rested; the weight measurements indicate how much water was in the vessel.

According to Trick [4], the flow meter measurements during the decreasing pressure phases are very noisy due to degassing effects. They have to be used with caution.

A comparison between the pressure evolution in BGS2 and the balance data indicated that the latter was not very accurate. This was confirmed by Nagra. It was found that

there was a weight increase during a pressure decrease, which is not plausible be-
cause the pressure decrease was caused by an outflow of water from the pressure
vessel.

Methods a) and b) provide independent flow data. The models are therefore calibrated
with regard to both pressure and flow measurements.
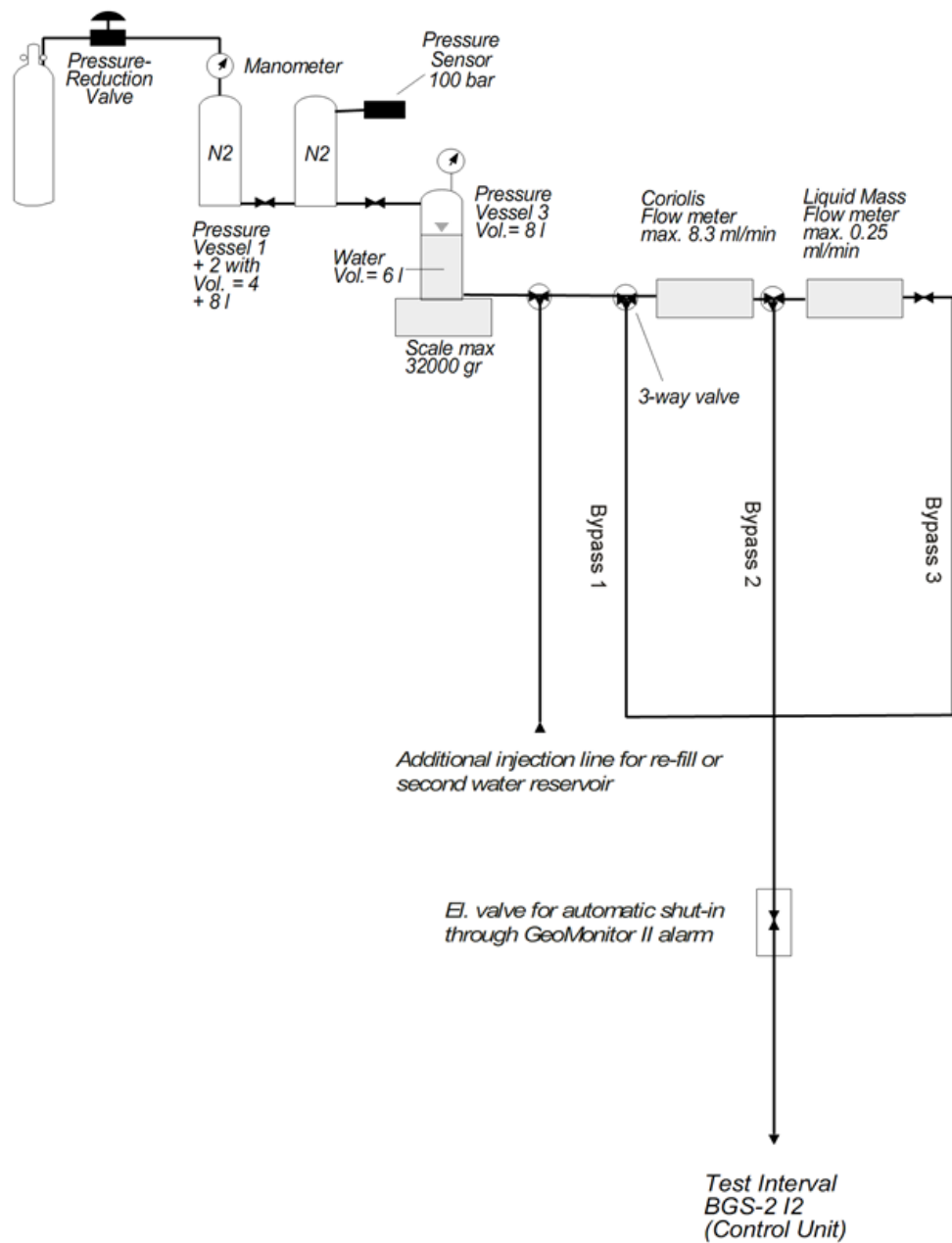
Fig. 3.1   Set-up of phase 1 of the HG-C experiment (taken from [4])
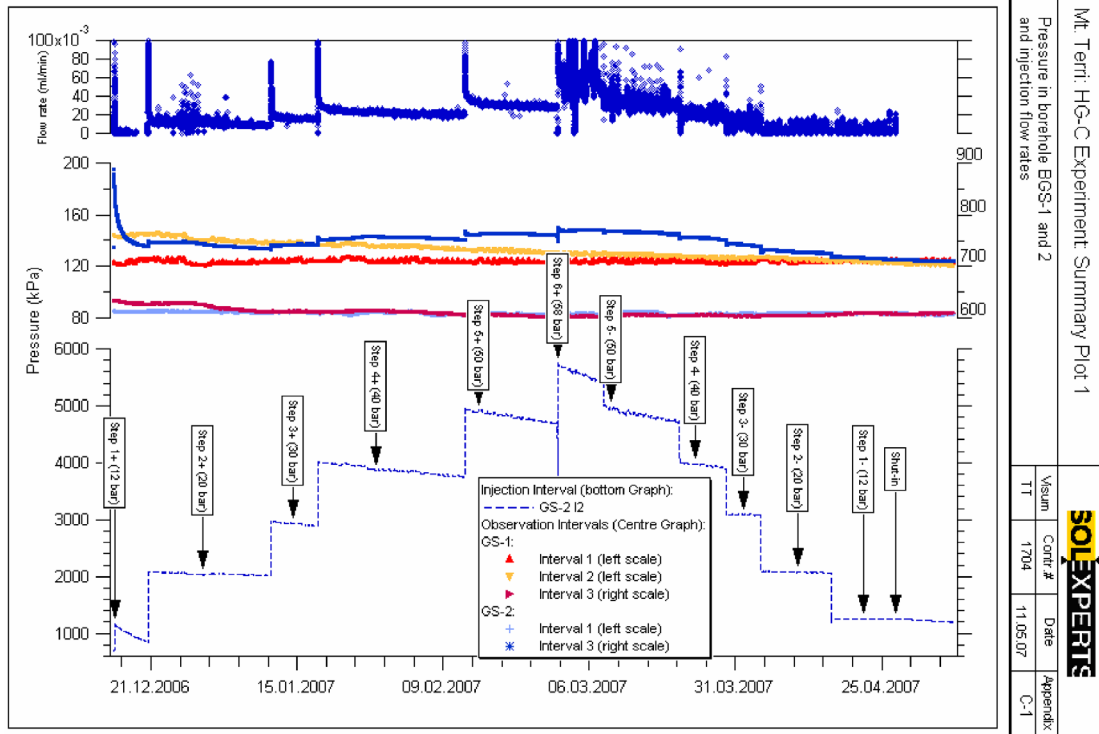
Fig. 3.2 Pressures and flows measured in the HG-C experiment (taken from [4])
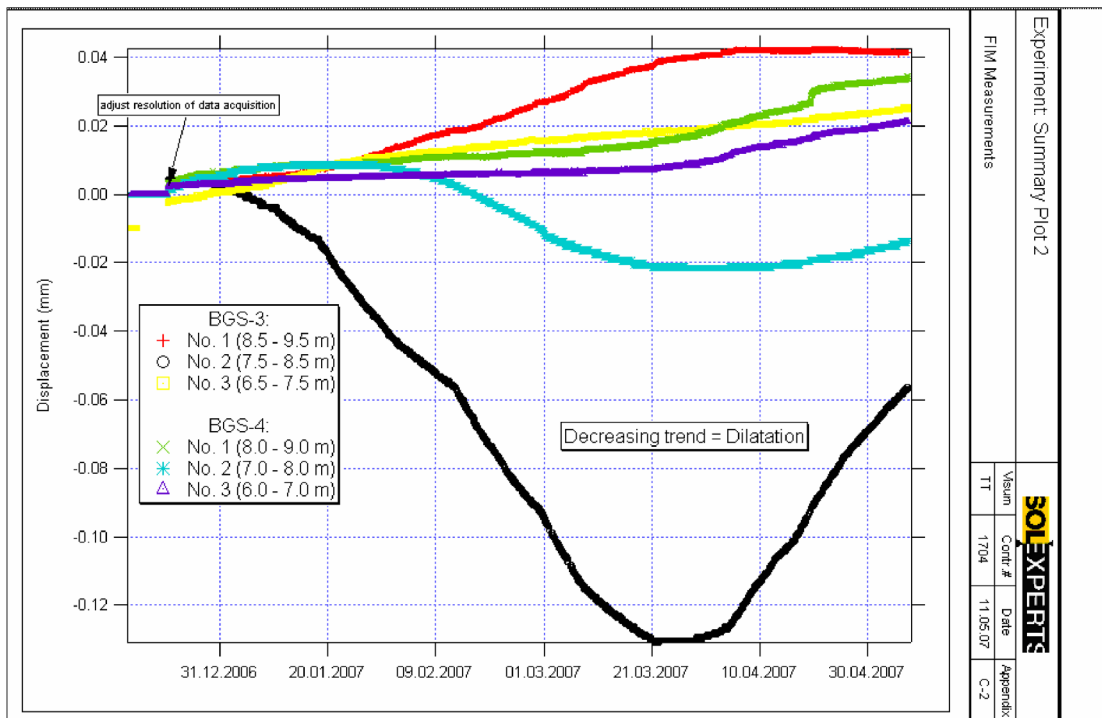
Fig. 3.3 Deformation measurements of the HG-C experiment (taken from [4])

3.2　Original TOUGH2 code

3.2.1　Modelling grid and boundary conditions

The geometry of the modelling grid is shown in Fig. 3.4 to Fig. 3.6.

In Fig. 3.4, the floor of the access shaft is represented by a blue horizontal rectangle at the top of the picture. The orientation of the boreholes is perpendicular to the bedding plane. Due to the symmetry of the set-up, only one half of the domain was modelled.

The pressure vessel and the piping were included in the model as a vertical column. The pressure vessel is represented by the upper part of the column, the piping by the lower part of the column. The piping was connected to interval 2 of BGS2 by an additional element connection. This connection exists in the TOUGH2 grid declaration only and cannot be seen in Fig. 3.4.

In the TOUGH2 grid declaration, the volume of element PIPE was set to 20 l in order to provide enough water for water injection. Fluid was injected from element PIPE to the injection interval via the element LINK which was placed in interval 2 of BGS2. Water injection was achieved by imposing a gas pressure on the pressure vessel VESS. This expelled water from the vessel, expanded the gas phase and reduced the vessel pressure.

All model faces are no-flow boundaries. This implies that flow into the rock requires compressibility effects.

Except for the injection interval (interval 2 of borehole BGS2), all packer intervals were represented by a single element (Fig. 3.5) in order to reduce calculation time. The interval volumes did not represent the actual volumes and were corrected in the TOUGH2 grid declaration.

Since the largest pressure gradients were expected in the vicinity of the injection interval, the radial grid was refined here (Fig. 3.6).[1]
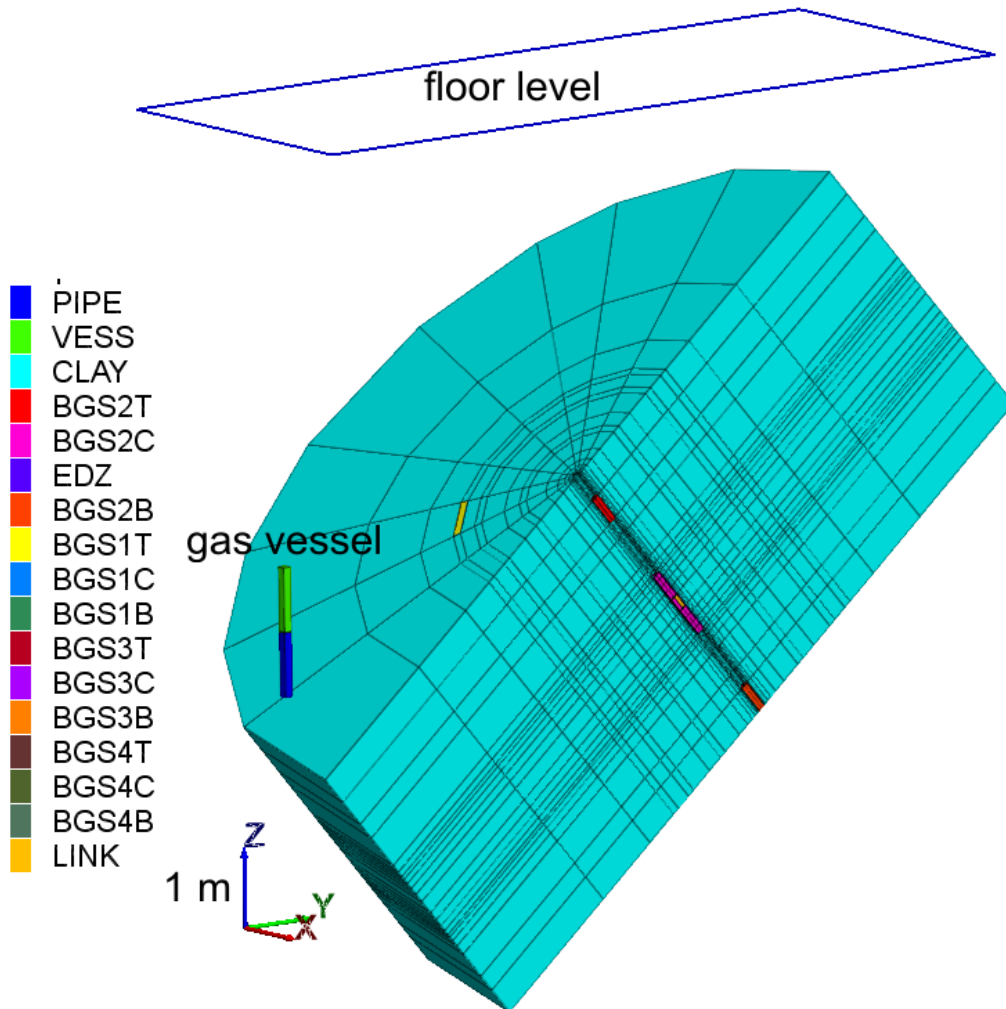
Fig. 3.4   Modelling grid for the simulation of the HG-C experiment with TOUGH2

Key explanation: Letters T, C, and B appended to the borehole names stand for "top", "centre", and "bottom", respectively. Thus, BGS2B stands for interval 1 of BGS2.

---

[1] A thin layer of 1 cm around the injection interval (named "EDZ") was introduced in order to keep the possibility of simulating a damaged zone. (Borehole damage zones were observed in some boreholes in Mont Terri). However, no use is made of this element layer in this study. Its properties are set to those of the intact clay.
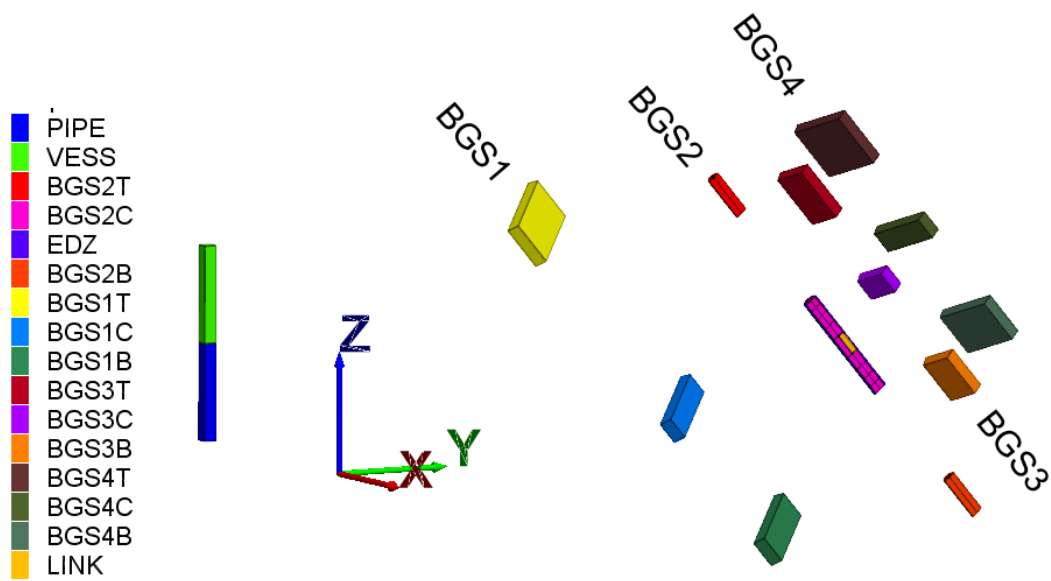
Fig. 3.5   Same view as in the previous Fig. but without the clay rock
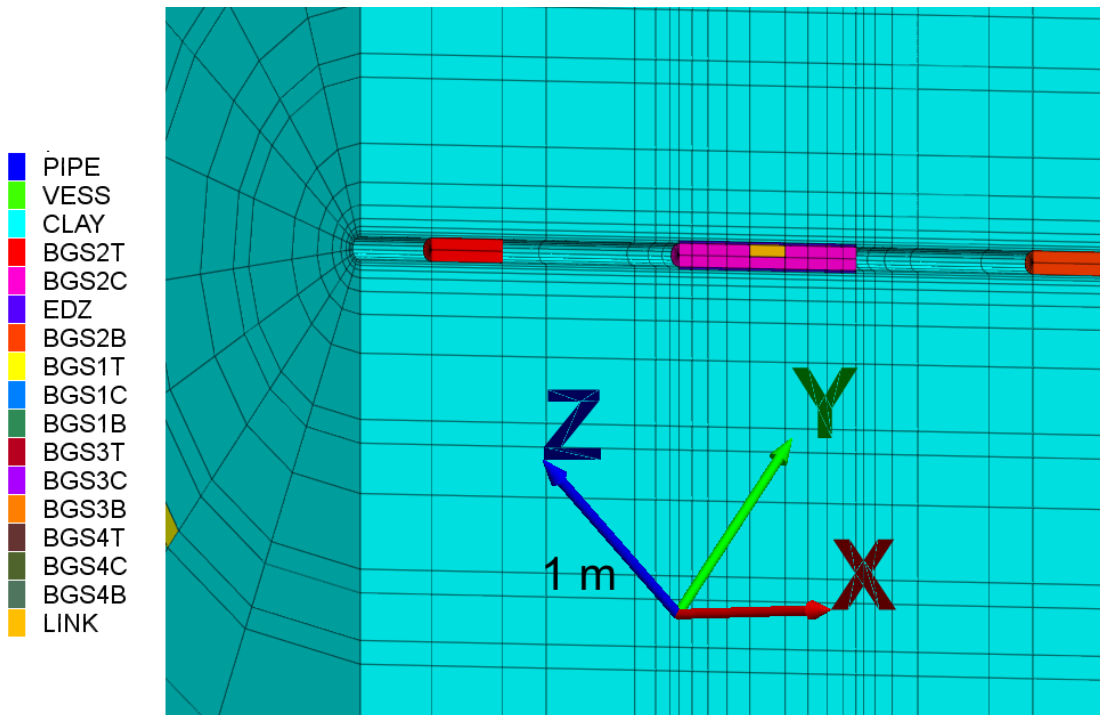
Fig. 3.6   Detail of the modelling grid showing the discretisation of the BGS2 borehole (The gas vessel is connected to interval 2 via the element "LINK")

3.2.2   Reference case

The reference case was based on information that was available at the beginning of the project. The reference case was used to analyse the principal behaviour of the system if two-phase flow is assumed.

The model system contains a liquid and a gas phase. The phases are composed of the components water and air (TOUGH2 was used in connection with the Equation-of-State module EOS7). Gas diffusion and heat transport were neglected. Tab. 3.1 shows the main parameter values of the reference case. The rock matrix was assumed to be compressible[2]. An approximate temperature of 10 °C was applied. Advective flux between two adjacent elements was calculated using the weighted harmonic mean of the intrinsic permeabilities and an upstream-weighted mobility[3]. Upstream-weighting of mobilities is necessary to allow the propagation of phase fronts.

The volume of the pressure vessel was corrected to account for the leakage that had probably occurred during pressure step 1+. During this step the pressure had dropped from 1.2 MPa to 0.847 MPa. Assuming that gas volumes and pressures change according to the ideal gas law, the initial gas volume of 2 l had probably increased to approx. 2.83 l during the leakage. Therefore, the vessel volume was set to 2.8 l in the model in order to achieve a realistic gas volume for the following pressure steps.

The results of the simulation are shown in Fig. 3.7 to Fig. 3.10 together with the measured data. Fig. 3.7 shows a good agreement of the simulated pressures and those pressures that were measured in interval 2 of BGS2 for the pressure steps 2+, 3+, 5+, 3-, 2-, and 1-. The pressure drop that has been measured during step 1+ was probably caused by a leakage. In the simulation, the pressure was set to the measured value at the beginning of each pressure step. The subsequent pressure drop reflected the evolution of the vessel pressure due to the expansion of the enclosed gas bubble.

---

[2] The TOUGH2 parameter "compressibility" C (the relative porosity change per pore pressure change) is calculated from the specific storage S_s by $C = S_s / (\phi \rho g) - c_l$, where ϕ is the porosity, ρ the density of water, g the gravitational acceleration and c_l the compressibility of water.

[3] In the language of TOUGH2 the term $k\, k_r/\mu$ is called "mobility", where k is the intrinsic permeability, k_r the relative permeability of the phase and μ is its viscosity.

In the simulation, no pressure signal was received in intervals 1 and 3 of boreholes BGS2 and BGS1 (Fig. 3.8). However, there was a pressure response in interval 2 of BGS1. The stronger reaction in the central interval of BGS1 (interval 2) probably attributes to the higher permeability parallel to bedding. The effect of anisotropy is also visible in the measured and simulated deformation in borehole BGS3 (Fig. 3.9). Both, simulation and measurements, show the strongest response in the central interval (interval 2), which probably attributes to the anisotropy that is introduced by the bedding of the clay.

Tab. 3.1   Parameters of the reference case (phase 1 of HG-C)

Parameter	Opalinus clay (shaly facies), EDZ, BGS3 and BGS4		Other packer intervals	pipe	vessel
intrinsic permeability	5 E-20 m² || bedding plane 5E-21 m² ⊥ bedding plane	Within range for shaly facies	1 E-15	1 E-15	1 E-15
porosity	0.13	0.10 to 0.16 [17]	0.95	0.95	1
Specific storage	1.5E-6 1/m	Estimation from preliminary Analyses (oral information by Nagra)	0	0	0
Relative permeability function	$k_{rl}=S^{*3}$ $k_{rg}=(1-S^*)^3$ $S^*=(S_l-S_{lr})/(1-S_{lr})$ $S_{lr}=0.001$	Power law with exponent between 2 and 3 reported for Callovo-Oxfordian clay	Same as for clay (less relevant)	as for clay (less relevant)	as for clay (less relevant)
Capillary pressure function	No capillary pressures	No gas phase injection into the rock in phase 1 of HG-C	No capillary pressures	No capillary pressures	No capillary pressures
Initial pressure for equilibration	0.68314 MPa	= pressure in BGS2-i2. Assumption: equilibrated with pore water pressure	0.68314 MPa (boundary condition for interval 2 of BGS2)	0.68314 MPa	0.68314 MPa
Initial pressure for HG-C phase 1	Result of equilibration		Result of equilibration	Result of equilibration	Result of equilibration
Initial gas saturation for equilibration	0.001	> 0 to avoid possible numerical problems in case of changes in the number of phases	0.001	0.001	0.001
Initial gas saturation for HG-C phase 1	Result of equilibration		Result of equilibration	Result of equilibration	0.999
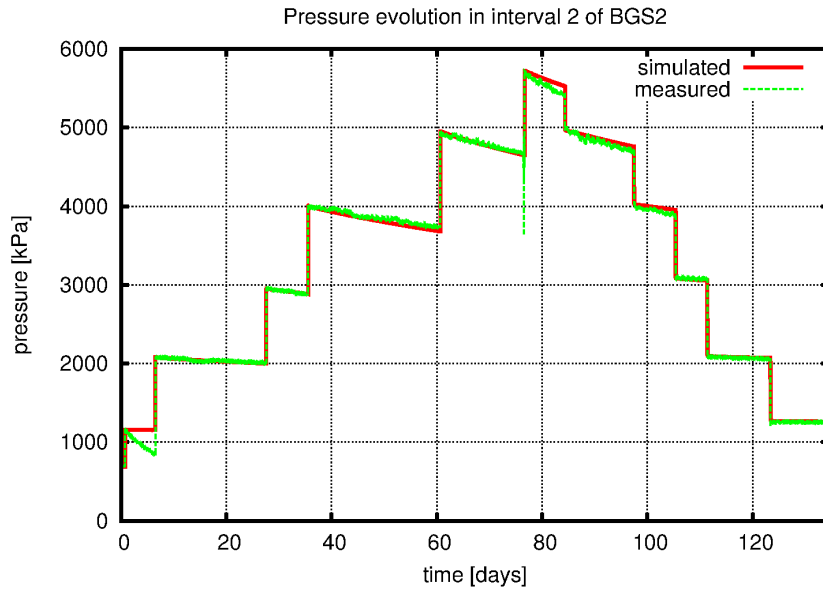
Fig. 3.7   Pressure in the injection interval of BGS2 (reference case)
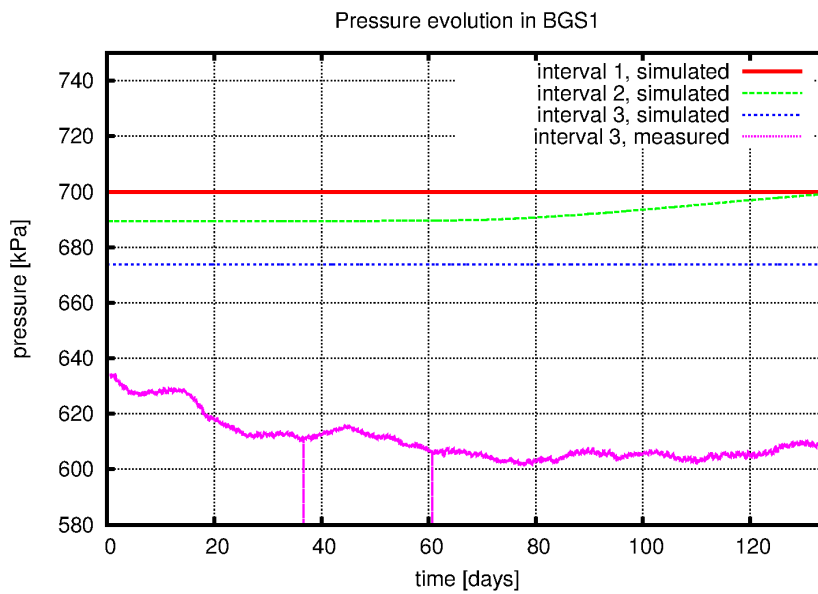
Fig. 3.8   Pressure response in BGS1 (reference case)

The measured pressure decrease in interval 3 might indicate a leakage or an incomplete equilibration with the pore water pressure of the rock.

16
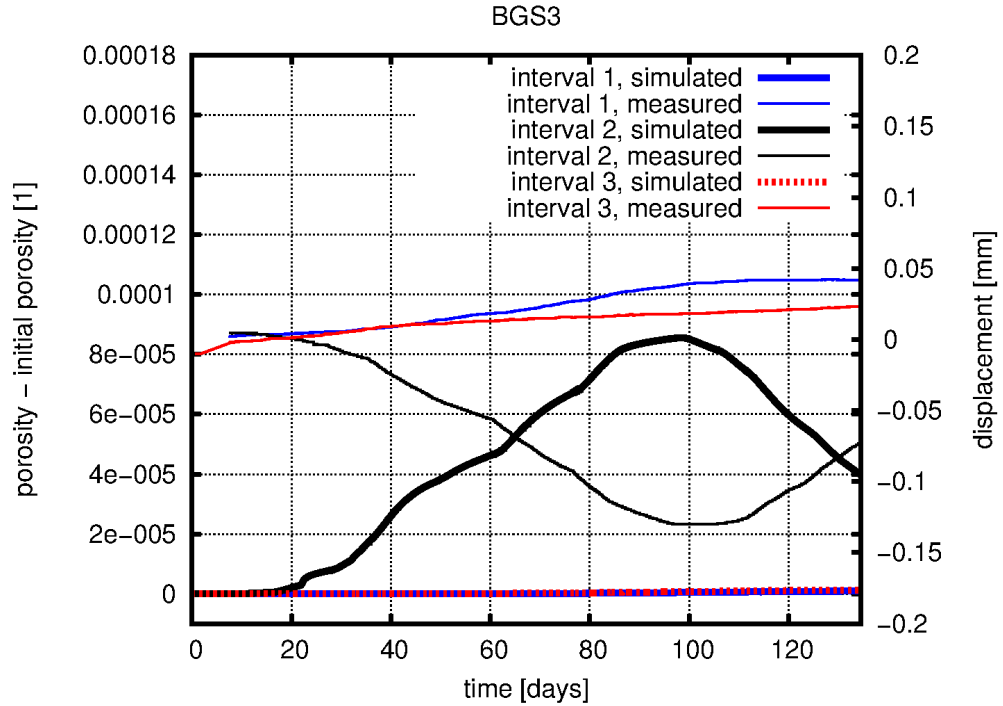
Fig. 3.9   Deformation in BGS3 (reference case)

> A decreasing trend of the displacement measurements stands for dilation. The measured
> dilation in interval 2 corresponds to a porosity increase in the simulation.

The simulated injection flows were considerably lower than the measured injection flows (see Fig. 3.10; "Qlow" denotes the measured data). This finding contradicts the quite good fitting results for the injection pressures (Fig. 3.7) because the pressure slopes are a direct consequence of the injection flows. This indicates that the gas volume inside the pressure vessel at the end of pressure step 1+ has been underestimated.
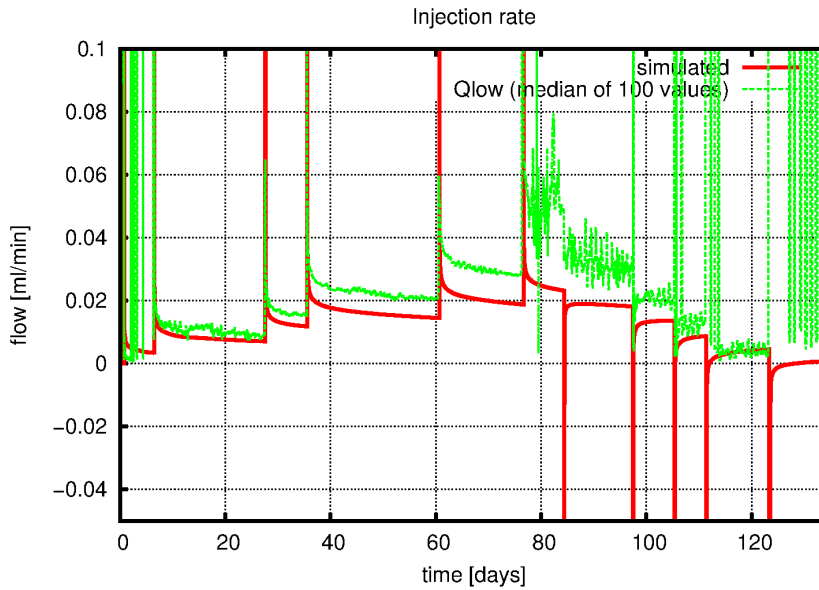
Injection rate

Fig. 3.10   Flow into the injection interval in the reference case

3.2.3   Parameter variation

The behaviour of the flow system at the HG-C site was investigated by varying single properties against the reference case.

3.2.3.1   Reducing porosity with constant specific storage

In this simulation case, the porosity of the clay was multiplied by a factor of 0.5 and the specific storage S_s was kept constant. Since the TOUGH2 parameter "compressibility"

$$C = S_s \,/\, (\phi\,\rho\,g) - c_l$$

depends on both porosity and specific storage, the compressibility of the clay had to be adapted to the new porosity.

The simulated injection pressures (Fig. 3.11) and injection flows (Fig. 3.12) did not show any deviation from the reference case. However, the reduced porosity caused a strong porosity increase in the central interval of the remote boreholes BGS3 and BGS1 (see Fig. 3.13 and Fig. 3.14). This can be explained by the reduced water volume inside the rock, which can be compressed in order to store additional water. The

18

constant specific storage guarantees a constant storage capacity of the rock so that the reduced effect of water compression had to be compensated by a higher porosity increase (i. e. matrix compression). For the flow process there is not much difference whether the space for the storage of additional water is provided by water or matrix compression. Therefore, a variation of porosity has no influence on water flow under saturated conditions provided that the specific storage is kept constant.
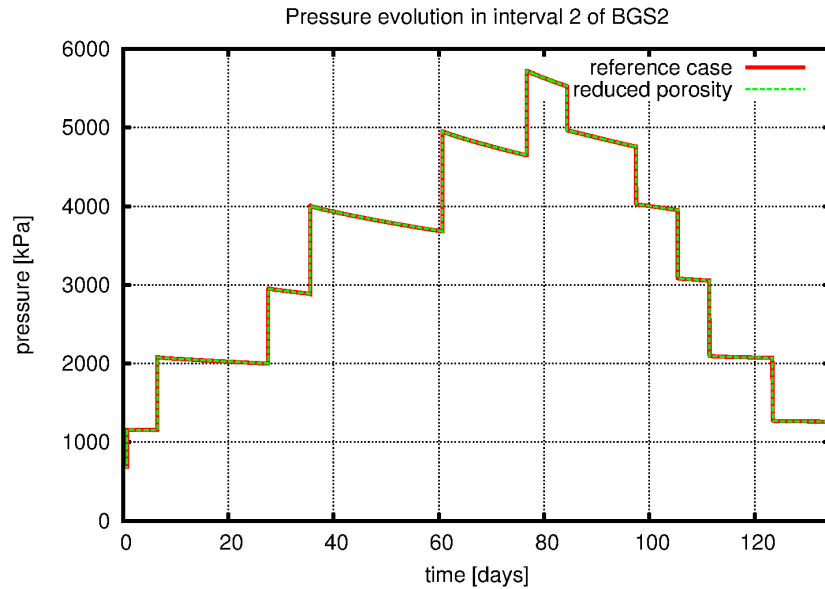
Fig. 3.11   Injection pressures
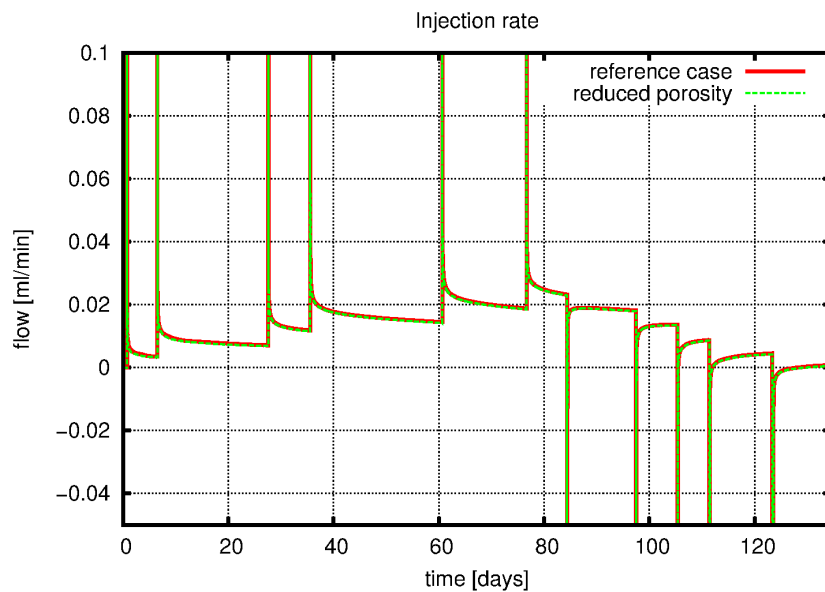
Fig. 3.12   Injection flows (interval 2 of BGS 2)
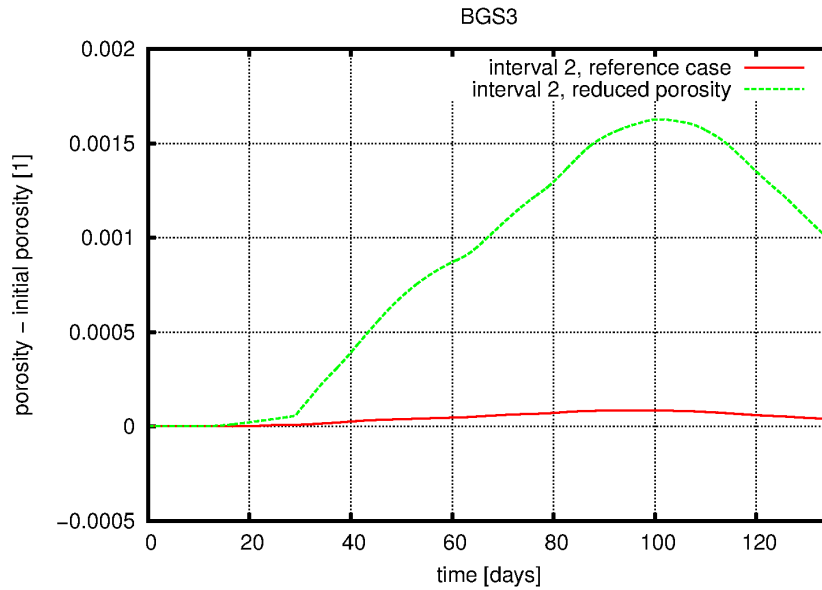
Fig. 3.13   Porosity change in interval 2 of BGS3
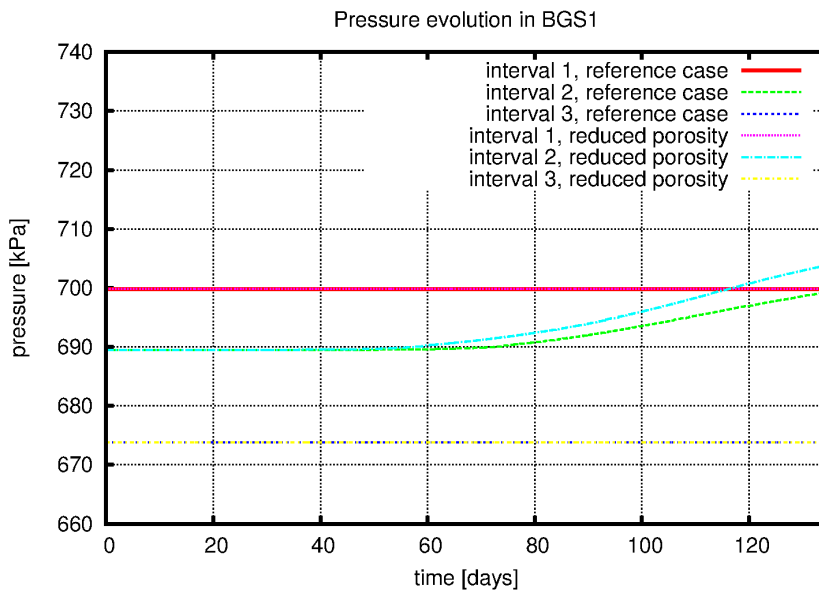
Fig. 3.14   Pressure response in BGS1

3.2.3.2   Increasing specific storage

Specific storage was increased by a factor of 10 in this simulation case. Fig. 3.15 shows slightly steeper pressure curves indicating higher injection flows. Fig. 3.16 confirms this observation. Flows are generally increased by a higher specific storage of the clay.
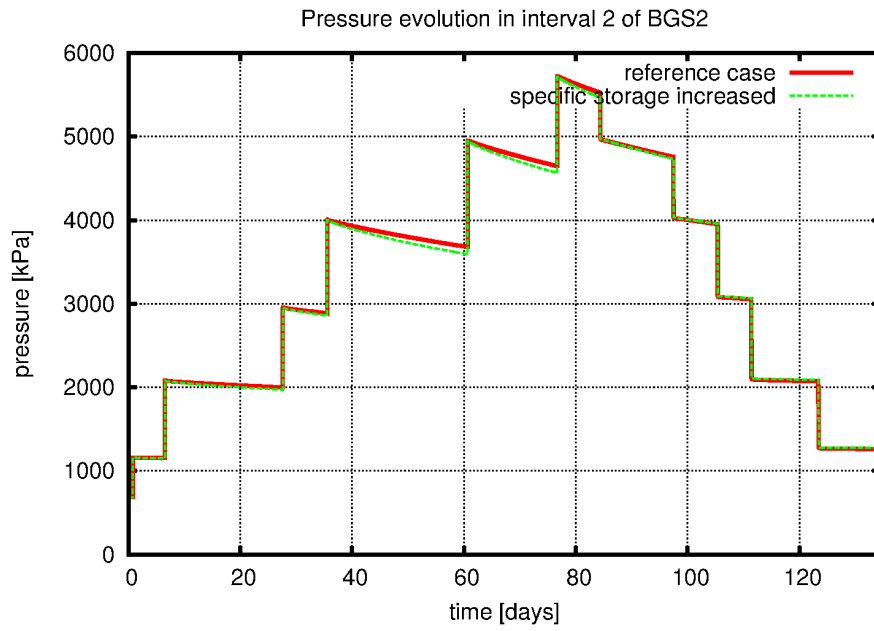
Fig. 3.15   Pressure evolution in interval 2 of BGS 2
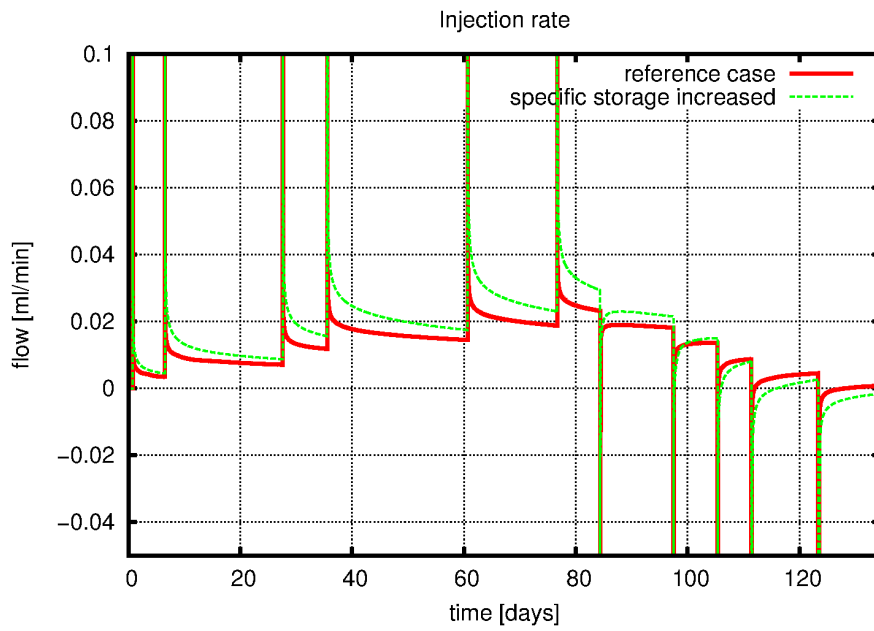
Fig. 3.16   Flow into interval 2 of BGS 2

21

The raised compressibility of the clay led to a stronger porosity increase in the central interval of BGS3 (Fig. 3.17). However, the pressure signal did not arrive at the more distant borehole BGS1 (Fig. 3.18). Probably, it was now possible to store most of the injected water in the vicinity of the injection interval due to the increased specific storage.
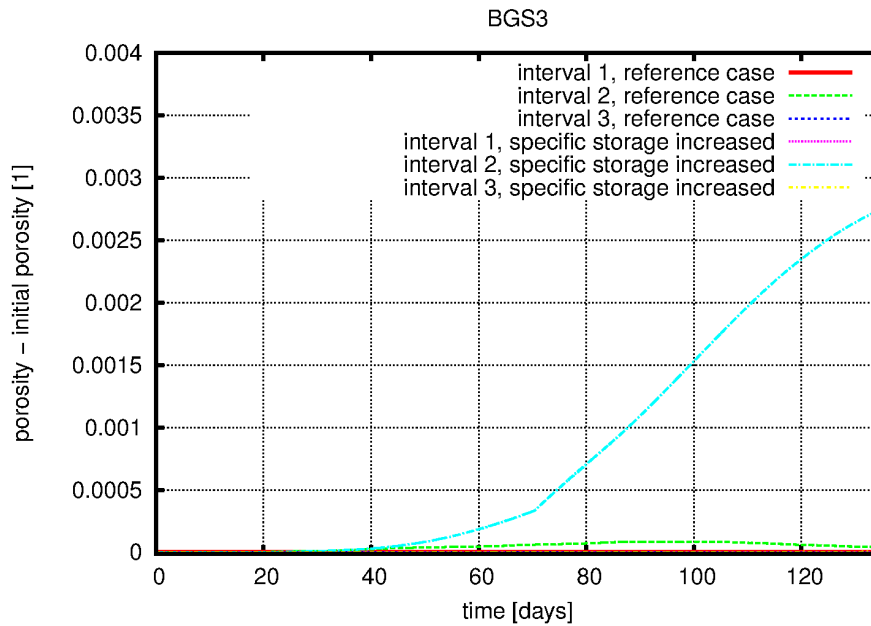
Fig. 3.17   Porosity change response in BGS 3
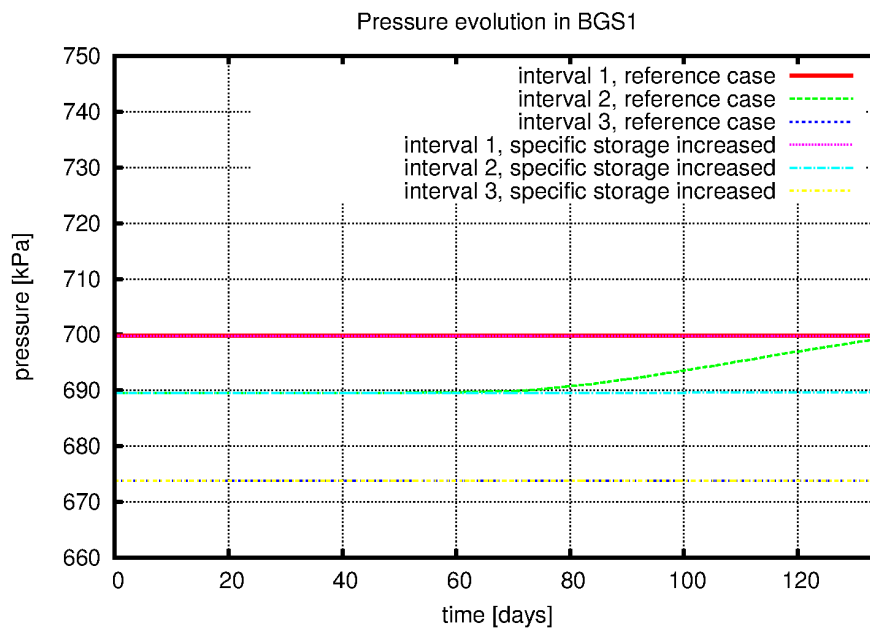
Fig. 3.18   Pressure response in BGS1

3.2.3.3 Increasing permeability

Horizontal and vertical permeabilities were doubled in this simulation case. This had a strong impact on injection pressures and flows. The slope of the pressure curves steepened (Fig. 3.19), injection flows increased (Fig. 3.20), and the central interval of BGS 1 experienced higher pressures (Fig. 3.21). A strong effect was also noticed in borehole BGS 3 (Fig. 3.22).
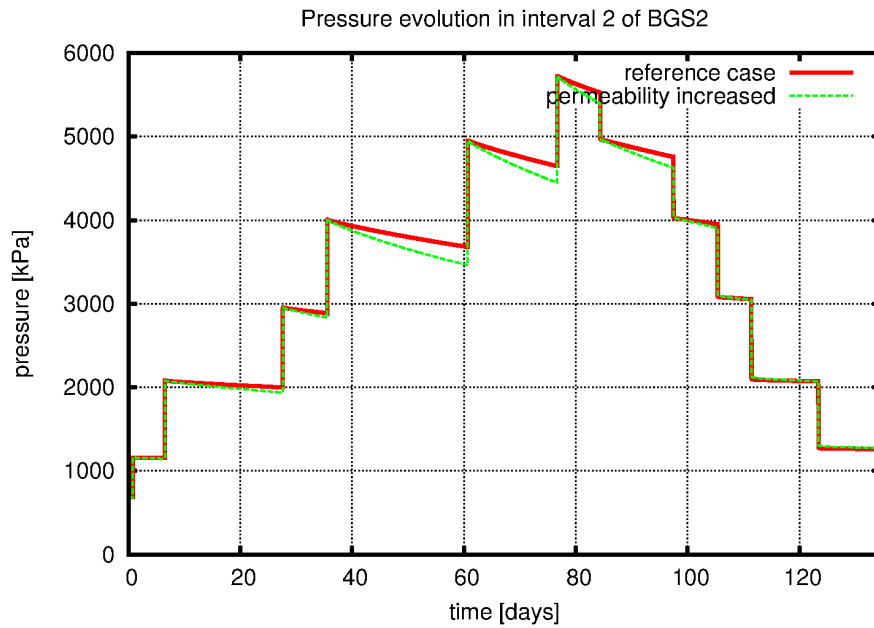
Fig. 3.19   Pressure evolution in interval 2 of BGS 2
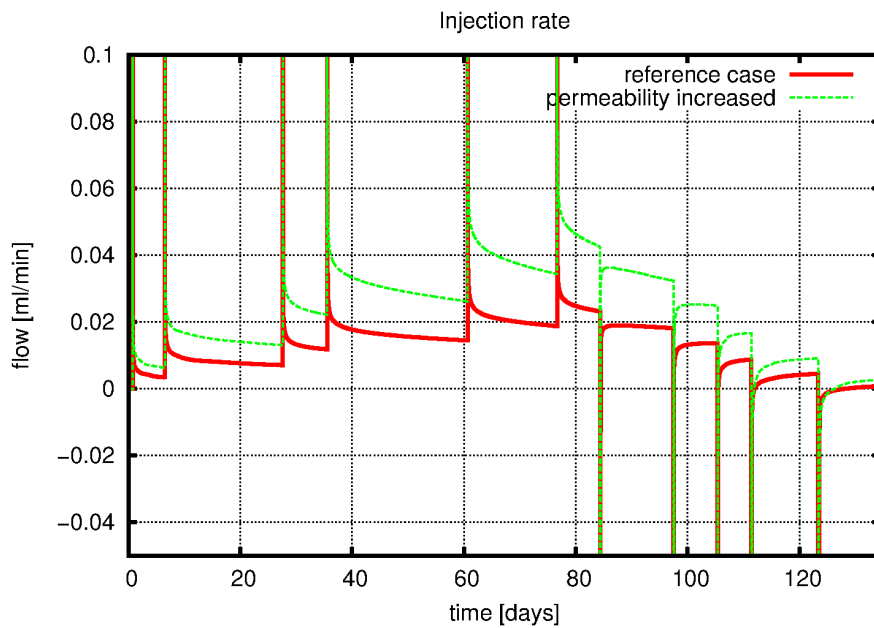
Fig. 3.20   Flow into interval 2 of BGS 2

23
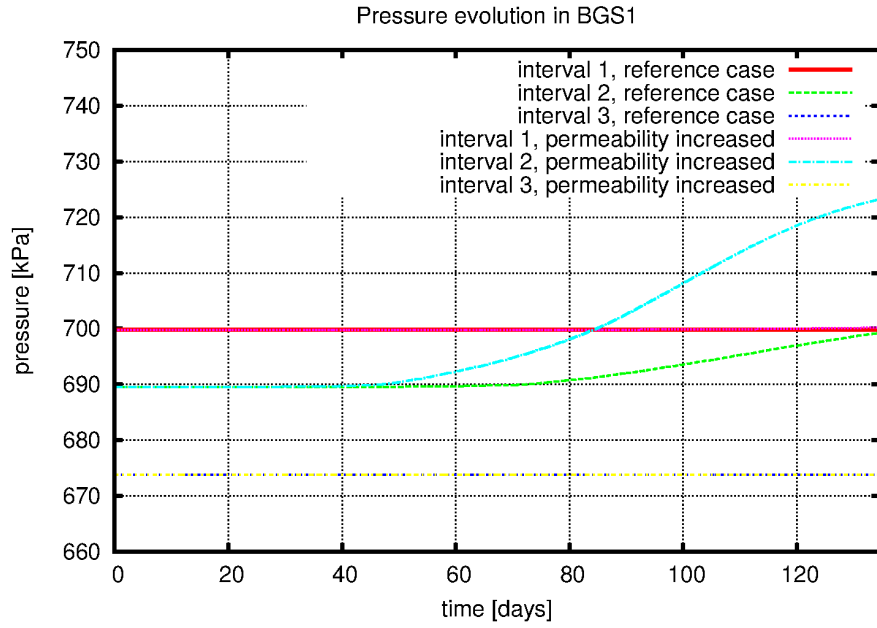
Fig. 3.21   Pressure evolution in BGS1
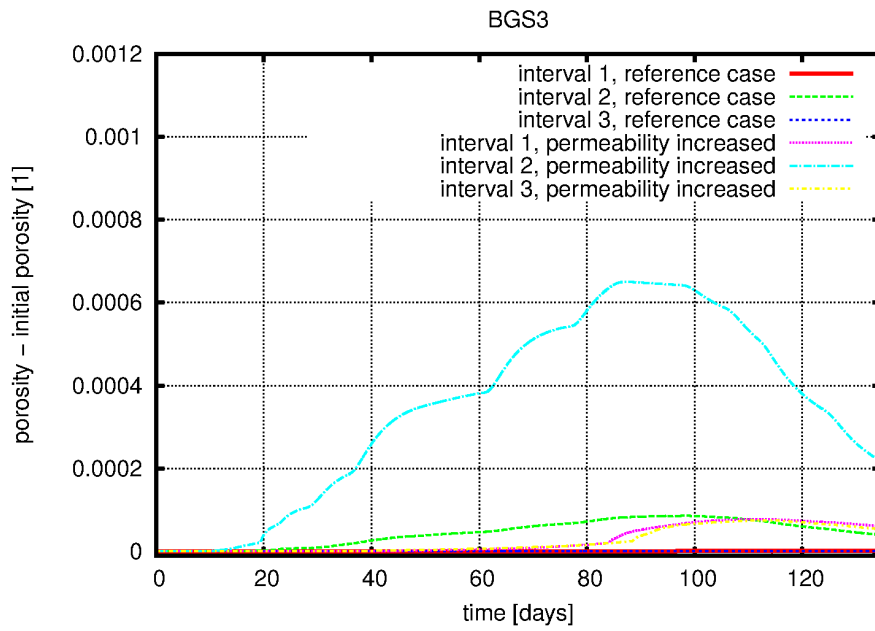
Fig. 3.22   Porosity change in BGS 3

3.2.4 Parameter fit

The previous analysis of the reference case indicated that the assumed initial gas volume of the pressure vessel was wrong. In order to fit injection pressures and injection flows at the same time, the initial gas volume of the pressure vessel was used as a fitting parameter.

Parameter fits were conducted on a trial-and-error basis with respect to both injection pressures and injection flows. The pressure data of BGS 1 was neglected because the data for the central interval was not reliable. Tab. 3.2 shows the results of the model calibration (other parameters according to the reference case).

With this parameterisation, the pressure curves agreed very well with the measurements of the pressure steps 2+, 3+, 4+, 5+, 3-, 2-, and 1- (Fig. 3.23). No satisfying fit was achieved for the highest pressure step (step 6+) and the subsequent steps 5- and 4-. The fit of the flow curves was significantly improved (Fig. 3.24) but of minor quality for steps 5+ and 5-.

The deviations observed at pressure steps 5- and 4- indicate the existence of a pressure threshold above which the injection of water was facilitated. For this reason a model with pressure-dependent permeability was developed (see the following section).

Tab. 3.2   Fitted parameters of the original TOUGH2 code for phase 1 of HG-C

Intrinsic permeability of clay, EDZ, BGS3 and BGS4	7.4 E-20 m² ‖ bedding plane 7.4 E-21 m² ⊥ bedding plane.
Initial volume of the gas vessel	5 liters
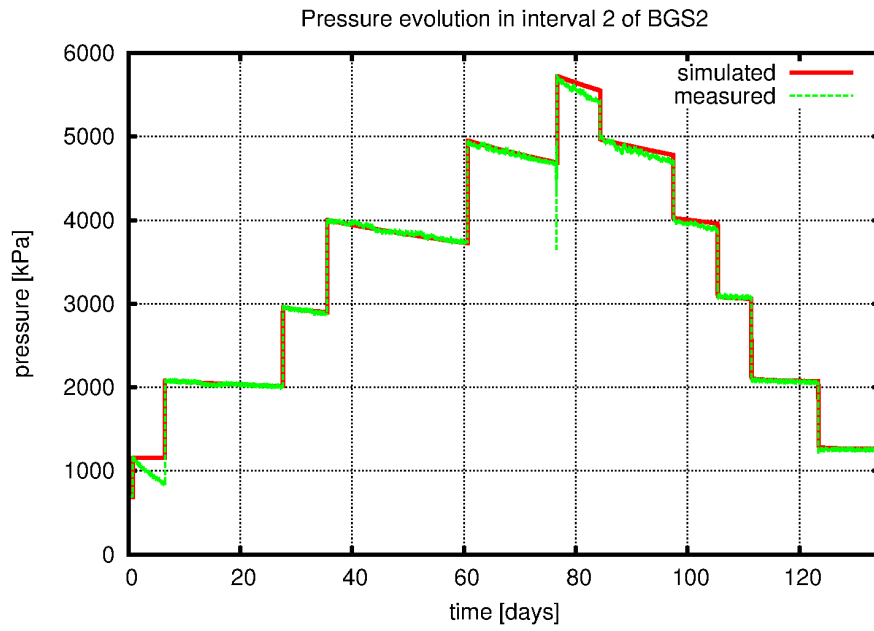
Fig. 3.23 Measured and fitted injection pressures (original TOUGH2 code)
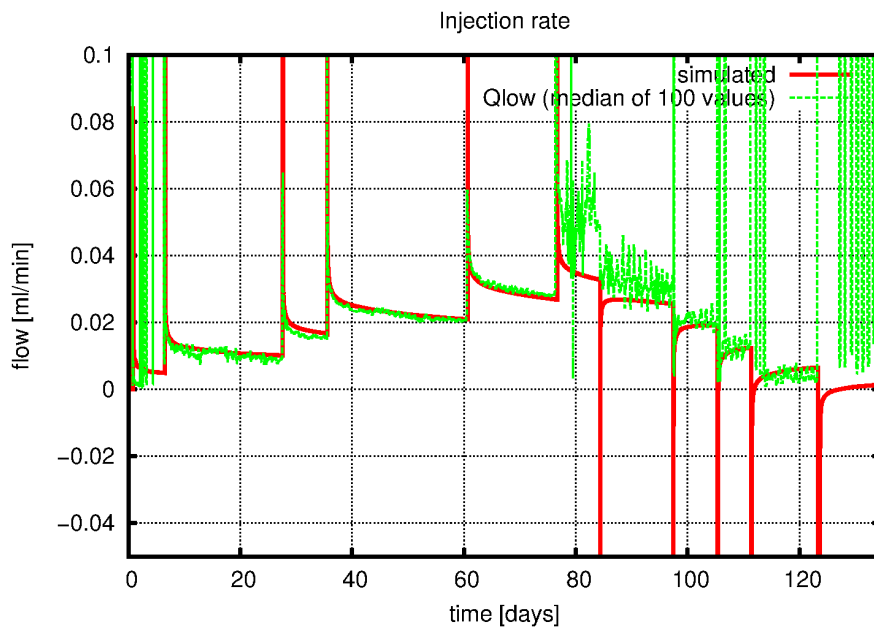
Fig. 3.24 Measured and fitted injection flows (original TOUGH2 code)

The noise in the measured flow data attributes to degassing effects

26

3.3 Variable permeability model

3.3.1 Model description

This model is a modified version of the TOUGH2 code. It is characterised by a pressure threshold above which permeability becomes pressure-dependent.

In TOUGH2, the flow F_β of phase β is determined by a generalised Darcy law

$$F_\beta = -k \frac{k_{r,\beta} \rho_\beta}{\mu_\beta} (\nabla p_\beta - \rho_\beta g) .$$

Here, k is the intrinsic and $k_{r,\beta}$ the relative permeability, ρ_β the density and μ_β the dynamic viscosity. g is the vector of gravitational acceleration and p_β the pressure of the phase. In the modified version of this equation, the relative permeability is multiplied by

$$\frac{p - p_{\text{thr}}}{p_{\text{ref}} - p_{\text{thr}}} \left(\frac{k_{\text{ref}}}{k} - 1 \right) + 1 , \text{ with } p_{\text{ref}} - p_{\text{thr}} \text{ and } k_{\text{ref}} > k$$

if $p > p_{\text{thr}}$. (The relative permeability is modified instead of the intrinsic permeability in order to have the modification in the upstream-weighted term of the flux equation.) Mobility thus increases linearly above the pressure threshold p_{thr} so that

$$k_{\text{ref}} \frac{k_{r,\beta}}{\mu_\beta} \quad \text{at} \quad p = p_{\text{ref}}.$$

The relative permeability is only modified in the direction parallel to the bedding. It was assumed that the anisotropic fabric of the clay facilitates crack opening and propagation in this direction.

3.3.2 Parameter fit

Using the variable permeability model, parameter fits were conducted with respect to the injection pressures and injection flows. The gas volume in the pressure vessel was used as an additional fitting parameter. Good curve fits were found using the parameters listed in Tab. 3.3.

Tab. 3.3   Fitted parameters of the variable permeability model for phase 1 of HG-C

Intrinsic permeability of clay, EDZ, BGS3 and BGS4	7.4 E-20 m² ‖ bedding plane 7.4 E-21 m² ⊥ bedding plane
Initial volume of the gas vessel	5 liters
p_{thr}	5 MPa
p_{ref}	6 MPa
k_{ref}	5 E-18 m²

The simulated injection pressures and injection flows are plotted in Fig. 3.25 and Fig. 3.26, respectively, together with the measured values. Both plots display a good curve fit. This applies especially to the highest pressure step (6+), for which no match was achieved with the original TOUGH2 code. The curve fits for the following two pressure steps (5- and 4-) are of minor quality, indicating the existence of irreversible or hysteretic processes.
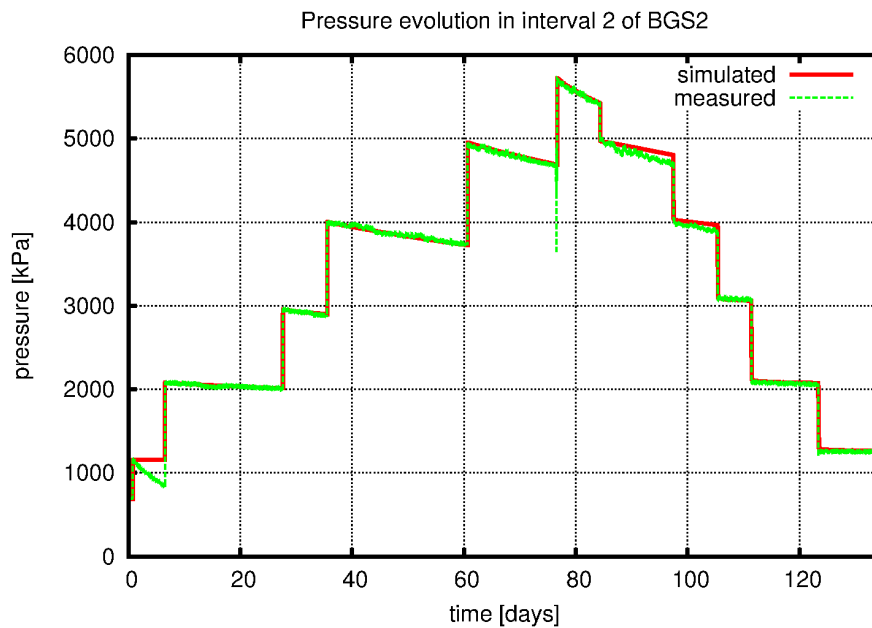
Fig. 3.25   Pressure in the injection interval of BGS2
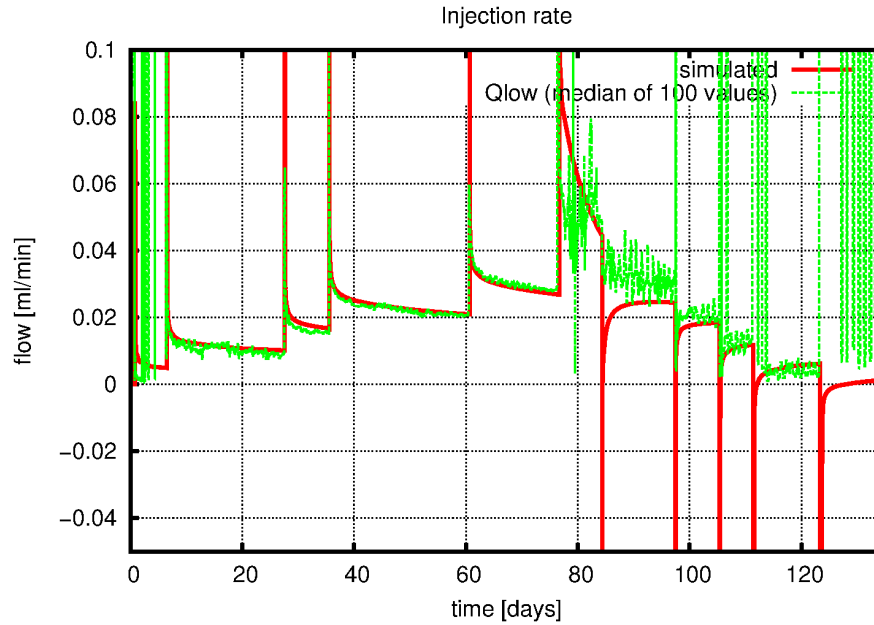
Fig. 3.26   Injection flow

The noise in the measured flow data attributes to degassing effects

3.4   Chapter summary

Phase 1 of HG-C was simulated assuming homogeneous properties of the host rock. The original TOUGH2 code was unable to reproduce the pressure and flow curves at the highest pressure step (step 6+). Better results were achieved using a modified version of TOUGH2 with variable permeability ("variable permeability model"). In this model, the mobility of water increases if a threshold pressure of 5 MPa is exceeded. This indicates the presence of pathway dilation in the experiment. However, both models were unable to reproduce steps 5- and 4-, which is an indication for irreversible or hysteretic processes.

The compression of the clay matrix as well as water compression were the main mechanisms for water uptake in the closed system. In the simulations, water injection rates depended strongly on the permeability of the clay. An increased specific storage led to higher injection rates, too, because it was now possible to store more water in the vicinity of the injection interval. This also reduced the travel distance of the pressure signal.

In order to calibrate the model against the injection pressures and injection flows at the same time, the initial gas volume of the pressure vessel had to be introduced as an additional fitting parameter. This is an indication of erroneous assumptions regarding the initial gas volume inside the pressure vessel or regarding the amount of gas leakage during pressure step 1+.

4 HG-C Phase 2 (gas injection)

4.1 Experimental results and data evaluation

Nagra provided the following raw data for the gas injection phase of the HG-C experiment (phase 2):

- Pressures in all packer intervals in kPa

- FIM measurements in BGS3 and BGS4

- Flow rates in nml/min. The gas flow was too low to be measured directly. Therefore the gas flow into the rock (not the one into the injection interval) was deduced from the decrease of the total gas volume inside the injection system and the pressure measurements by Solexperts.

Nitrogen has been used for gas injection. In the experiment, the injection pressure was increased in five steps. During each pressure step the gas pressure vessel was shut-in.

Fig. 4.1 shows the pressure evolution in the three intervals of the injection borehole. Interval 3 of the injection borehole responded very fast to the first pressure step, which might be an artificial effect. Incomplete sealing was detected for interval 1 of BGS1 and interval 1 of BGS2. The pressure measurements for these intervals were therefore dismissed. Fig. 4.2 shows the experimental set-up.
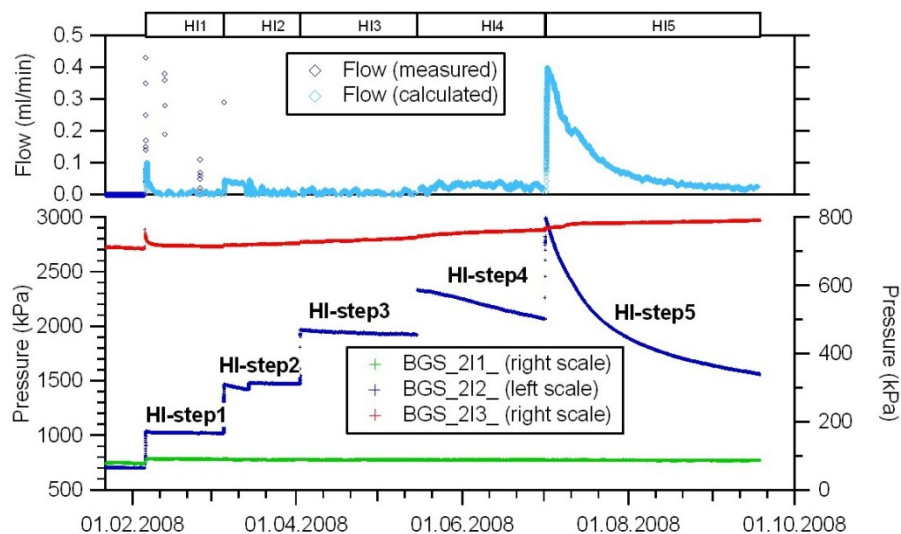
Fig. 4.1   Pressures in the three intervals of borehole BGS2 (taken from [5])
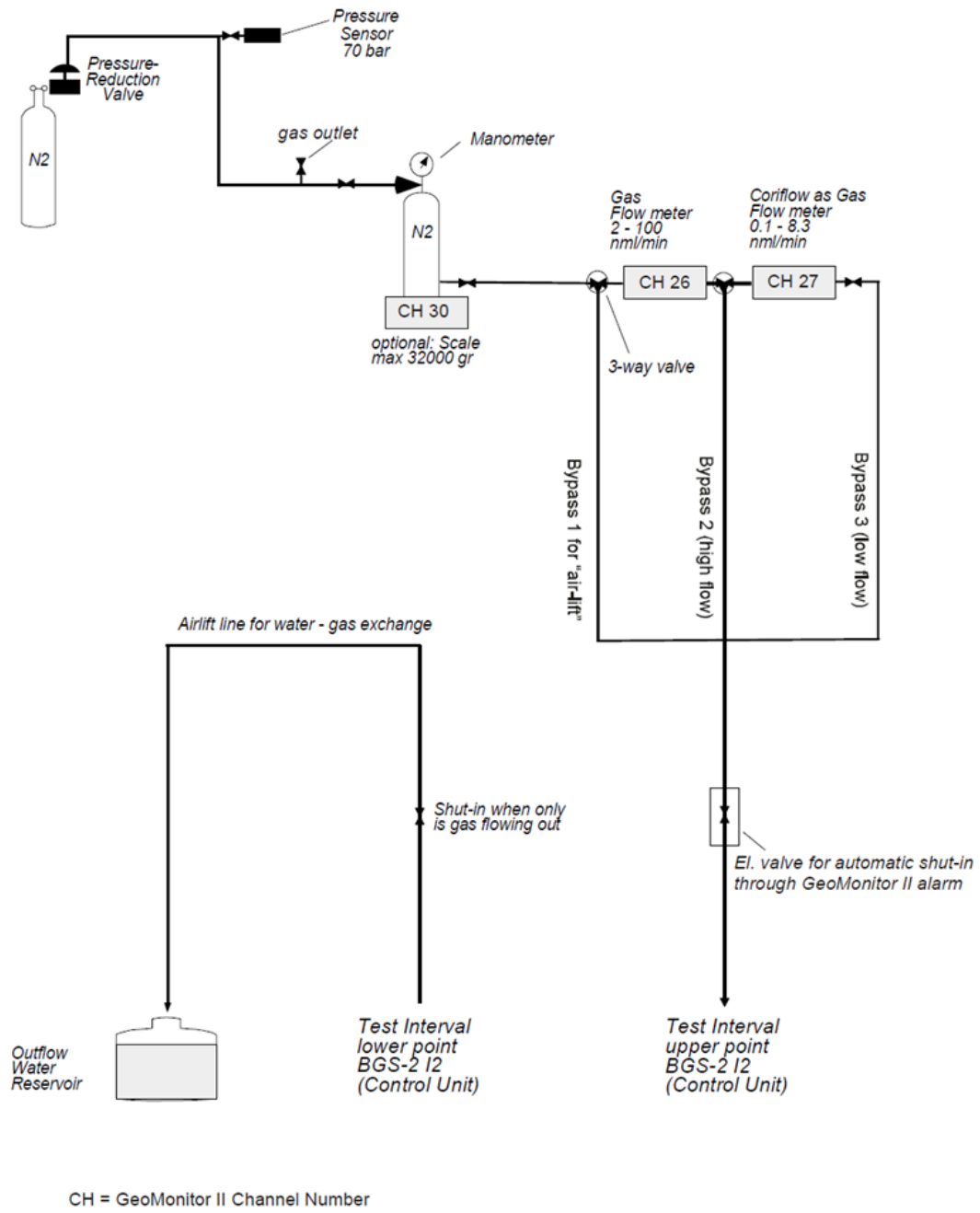
Fig. 4.2 Experimental set-up of the HG-C gas tests (taken from [5])

4.2　　　　Applying the variable permeability model

Phase 2 was first simulated with the variable permeability model, which had also been applied for phase 1 (section 0). The same model grid and parameters were used. For phase 2, the injection interval was completely desaturated in the model. The molar mass of the gas component was set to that of N_2.

As the gas volume in the experimental devices was unknown, the injection pressure was set as a time-dependent boundary condition (i. e. the injection pressure did not depend on the injection flow). The injection flows were used for model calibration. In the following, all gas flows refer to volume flows that are normalised with regard to the reference condition of 0.1 MPa and 21° C.

The modelling results show a striking difference between the simulated and measured injection flows (Fig. 4.3). Only small flow peaks were produced by the model. This might attribute to the low relative gas permeability of the almost saturated rock and to the fact that water has to be flushed out of the rock in order to gain space for the entering gas phase, which does not seem to be an effective mechanism for gas entry.

Apparently, the variable permeability model was not able predict the gas injection phase of the HG-C experiment. Therefore, alternative models were developed for this test phase.
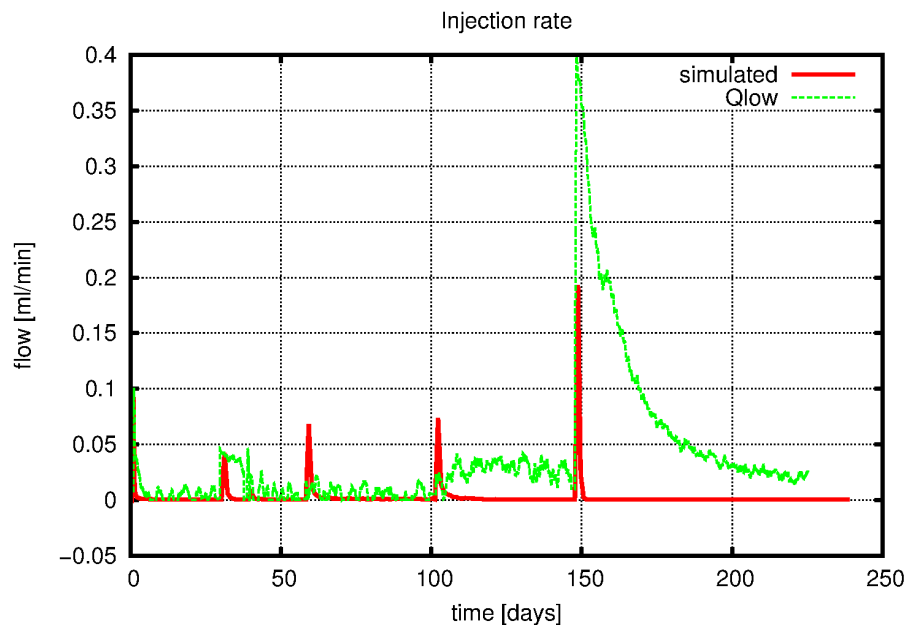
Fig. 4.3　　Injection flows

4.3 Pathway dilation model

In the HG-C experiment, gas injection was dominated by thresholds. According to Fig. 4.4 the main gas entry event started on day 147 (pressure step HI5) with a precursory gas flow, which set in on day 100 (pressure step (HI4). This indicates that the initial threshold for the main gas entry ranged between 2.34 MPa and 3 MPa at the site. In view of the findings described in the previous section it is unlikely that gas entered by displacement of water from saturated pores. More likely is a pressure-driven dilation of pathways.

As shown by Fig. 4.4, gas was still injected on day 225 although the injection pressure had already dropped to 1.57 MPa, i. e. below the initial threshold for gas entry. If pathway dilation indeed was the main mechanism for gas entry then the process clearly had irreversible or at least hysteretic components.

In this study, models with pressure-dependent permeability, porosity and gas entry threshold were tested. Yet, none of these models was capable of creating and maintaining a low pressure regime in the rock, which would allow for the observed long-lasting injection flow. This suggested the presence of an additional mechanism for pressure reduction inside the rock. These considerations gave rise to the formulation of a pathway dilation model, which introduces a pressure-dependent rate of porosity change ("dilation rate"). With a positive dilation rate, pressures are successively reduced in the rock due to an expansion of the contained gas phase. This allows the uptake of gas over long periods of time. The TOUGH2 code was extended to implement this model.
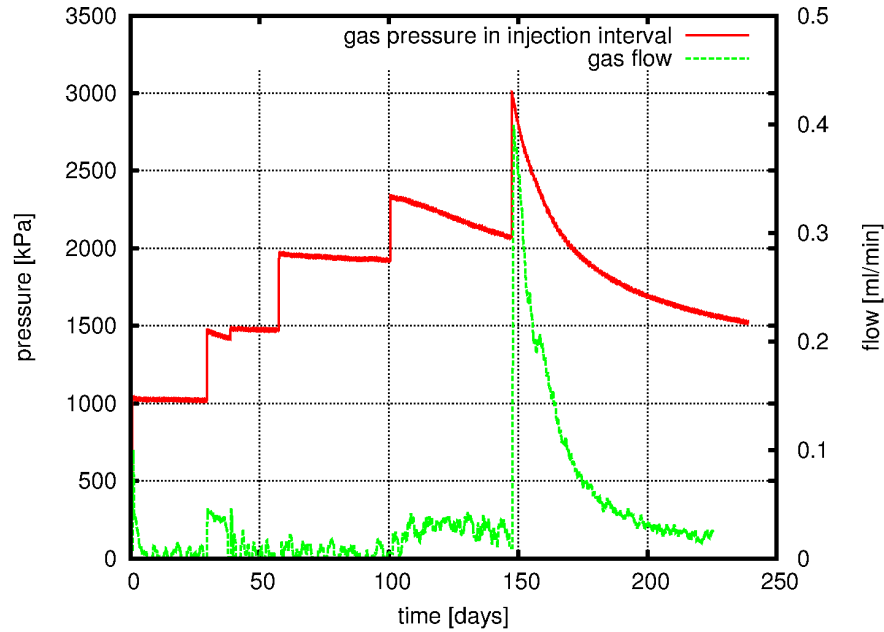
Fig. 4.4   Measured injection pressures and injection flows (phase 2 of HG-C)

4.3.1   Conceptual model

It is assumed that micro cracks open in the rock if the pore pressure exceeds a certain pressure threshold. The aperture of the cracks depends on pore pressure. The opening of cracks causes a macroscopic dilation of the rock.

The crack network shall be divided into main flow paths and dead end branches (see Fig. 4.5). The opening of dead end branches shall be a time-dependent relaxation process causing the mean porosity to increase with time. The macroscopic permeability shall be controlled by those parts of the crack network that constitute the main flow paths. Since the number of main flow paths shall not increase with time and crack apertures are in equilibrium with pressure, the macroscopic permeability is only pressure-dependent but not explicitly time-dependent. Permeability and porosity are independent in this crack network model.

This gives rise to the following conceptual model:

- There is a threshold pressure p_{thr} below which the main flow paths are closed. This means that the permeability component which attributes to the crack network vanishes for pore pressures below the threshold pressure.

- For a pore pressure $p > p_{\text{thr}}$, the pressure threshold p_{thr} decreases from an initial value p_{thr}^0 to a lower limit $p_{\text{thr}}^{\text{min}}$ with increasing pressure p (irreversible softening against microscopic tensile failure).

- Gas permeability is anisotropic and increases linearly with pressure difference $p - p_{\text{thr}}$. There is no gas permeability if $p < p_{\text{thr}}$.

- Porosity is variable and time-dependent. Porosity change is governed by a "dilation rate" $d\phi_{\text{dil}}/dt$, which increases linearly with $p - p_{\text{thr}}$ and becomes zero for pressures below the current threshold pressure. This implies that, except for $p \leq p_{\text{thr}}$, porosity grows steadily. Yet, the system equilibrates because the gas phase inside the pores expands due to the dilation of the rock causing a decrease of pore pressure. This process continues until the pore pressure reaches the threshold pressure p_{thr} so that the dilation process stops.
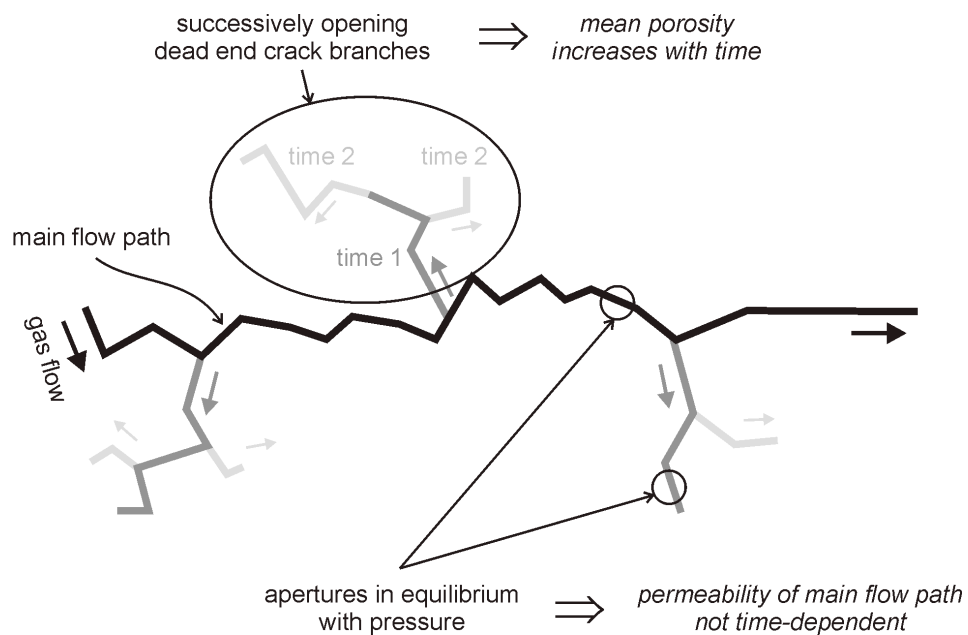
Fig. 4.5   Conceptual model of the dilation process

Rock dilation is caused by a pressure-induced opening of crack networks (black and grey lines). The mean permeability of the rock is controlled by the apertures of those cracks forming main flow paths (black line). Since crack apertures are expected to be in equilibrium with pressure, permeability is not expected to be explicitly time-dependent. Permeability is therefore defined as a pressure-dependent function in the model. Over time, dead end crack branches open (lines in dark and light grey). This relaxation process continuously increases the mean porosity of the rock but does not affect permeability. The time-dependent increase of porosity is described by a pressure-dependent rate of porosity increase ("dilation rate") in the model.

The time-dependent increase of porosity reflects a time-dependent damage to the rock on the micro-scale. The model is only applicable for a low degree of damage and crack connectivity so that dead end crack branches can still exist. This should be reflected in porosities remaining well below 1 during the equilibration process.

It is likely that most of the pore water is not in direct contact with micro cracks. In order to avoid overestimation of phase interactions, the following simplifying assumptions were made:

- water is immobile

- water is not compressible

- no gas is dissolved in the water.

Also, the compressibility of the matrix was set to zero to clarify the effects of pathway dilation. With all these assumptions the system virtually is a one-phase flow system.

4.3.2　　　Mathematical model

In the model, irreversible softening against microscopic tensile failure is achieved by reducing the threshold pressure p_{thr}. p_{thr}^i is the threshold pressure at time step i, with $i = 0$ at the beginning of the simulation. p_{thr}^i is defined by means of a pressure $\hat{p}_{\mathrm{thr}}$, which is the threshold pressure that would develop in undisturbed rock by applying pressure p:

$$\hat{p}_{\mathrm{thr}} = \frac{p - p_{\mathrm{thr}}^0}{p_{\mathrm{soft}} - p_{\mathrm{thr}}^0}\left(p_{\mathrm{thr}}^{\mathrm{min}} - p_{\mathrm{thr}}^0\right) + p_{\mathrm{thr}}^0 \quad \text{for} \quad p_{\mathrm{soft}} \geq p \geq p_{\mathrm{thr}}^0$$

$$\hat{p}_{\mathrm{thr}} = p_{\mathrm{thr}}^{\mathrm{min}} \quad \text{for} \quad p > p_{\mathrm{soft}}$$

$$\hat{p}_{\mathrm{thr}} = p_{\mathrm{thr}}^0 \quad \text{for} \quad p < p_{\mathrm{thr}}^0 \,.$$

$\hat{p}_{\mathrm{thr}}$ decreases from p_{thr}^0 to $p_{\mathrm{thr}}^{\mathrm{min}}$ as p rises from p_{thr}^0 to p_{soft}. An irreversible softening can now be introduced by

$$p_{\mathrm{thr}}^i = \min\left(p_{\mathrm{thr}}^{i-1}, \hat{p}_{\mathrm{thr}}\right).$$

The flow equation of TOUGH2 was replaced by the following equation in order to implement the effect of pathway dilation on the mobility of the gas phase:

$$
F_{\text{gas}} = -\left(\underbrace{\frac{\rho_{\text{gas}}}{\mu_{\text{gas}}} k\, k_{\text{r,gas}} \mathbf{I}}_{\substack{\text{determines the gas flux} \\ \text{in the original pore space}}} + \underbrace{\frac{\rho_{\text{gas}}}{\mu_{\text{gas}}} \mathbf{K}_{\text{dil}} k_{\text{dil}}}_{\substack{\text{determines the gas flux} \\ \text{in the additional pore space} \\ \text{created by pathway dilation}}} \right) (\nabla p_{\text{gas}} - \rho_{\text{gas}} g).
\tag{4.1}
$$

Here, k is the intrinsic and $k_{\text{r,gas}}$ the relative gas permeability, ρ_{gas} is the density, μ_{gas} the dynamic viscosity of the gas phase, and g the vector of gravitational acceleration. k_{dil} is a pressure-dependent gas permeability of dilated pathways. The tensor $\mathbf{K}_{\text{dil},i}$ introduces anisotropy. The two terms in the large brackets of equation (4.1), which determine the gas flow in the orginal pore space and in the pore space gained by pathway dilation, can be weighted separately in the spatially discretised equation. The term for the dilated pores is always upstream-weighted.

The permeability of the pore space gained by dilation k_{dil} was defined by the relationship

$$
k_{\text{dil}} = \left(p - p_{\text{thr}}^i \right) C_1 \quad \text{for} \quad p \geq p_{\text{thr}}^i
$$

where C_1 is a calibration parameter. If the pressure is below the threshold pressure, k_{dil} is zero.

Porosity ϕ was defined as the sum of the initial porosity ϕ_0 and the porosity gained by dilation ϕ_{dil}:

$$
\phi = \phi_0 + \phi_{\text{dil}} \quad \text{with} \quad \phi_{\text{dil}} = 0 \quad \text{for} \quad t = 0.
$$

ϕ_{dil} is called "secondary porosity" in the following. The change of ϕ_{dil} is controlled by the equation

$$
\frac{d\phi_{\text{dil}}}{dt} = \left(p - p_{\text{thr}}^i \right) C_2 \quad \text{for} \quad p \geq p_{\text{thr}}^i.
\tag{4.2}
$$

If the pressure is below the threshold pressure, $\frac{d\phi_{\text{dil}}}{dt}$ is set to zero. The pathway dilation model is now parameterised by the six parameters $C_1, C_2, p_{\text{thr}}^0, p_{\text{thr}}^{\text{min}}, p_{\text{soft}},$ and $\mathbf{K}_{\text{dil}}$.

In order to achieve a 1-phase flow system, water was immobilised by setting the permeability of the original pore space k to zero. A flow of gas can therefore only establish itself by pathway dilation.

In order to eliminate gas storage by processes other than pathway dilation, the density of water was kept constant and the solubility of the gas component in the liquid phase was set to zero. This way, neither water compression nor gas dissolution can take place. (The consequences of water compression and gas dissolution are described in section 4.4.)

In order to eliminate further gas storage effects, the initial pressure of non-dilated grid elements was set to 1000 Pa below the initial threshold pressure. This prevents that significant amounts of gas have to flow from dilated to non-dilated grid elements in order to raise the pore pressure to the initial threshold pressure for dilation. Such a flow would take place because of the small gas saturation of approximately 10^{-5} that was introduced as an initial condition for numerical reasons[4]. Without raising the initial pressure to close to the initial threshold pressure, the initial gas saturation would provide an artificial storage for gas. The elevated initial pressure does not cause any artificial flow between non-dilated elements because the permeability of non-dilated elements is zero.

---

[4]   In the simulations, the initial gas saturation was much smaller than the porosity changes caused by dilation.

4.3.3 Parameter fit

The dilation model was calibrated with the aim to fit the injection flows to the measured flow data. Satisfactory fits were achieved with the parameter set displayed in Tab. 4.1.

The results of the best-fit calculation are plotted in Fig. 4.6. The time axis ranges from day 90 to day 240 and covers the pressure intervals HI4 (starting on day 100) and HI5 (starting on day 147). In the experiment, a small flow of gas has been detected in step HI4 which was not reproduced in the simulation. However, there is quite good agreement for interval HI5.

Tab. 4.1   Fitted parameters of the dilation model for phase 2 of HG-C

C_1	2.1E-27 m²/Pa
C_2	5E-17 sec^{-1}Pa^{-1}
p_{thr}^0	2.35 MPa
p_{thr}^{min}	1.1 MPa
p_{soft}	2.4 MPa
K_{dil}	$(1, 1, k_3)$ with $k_3 = 0.1$
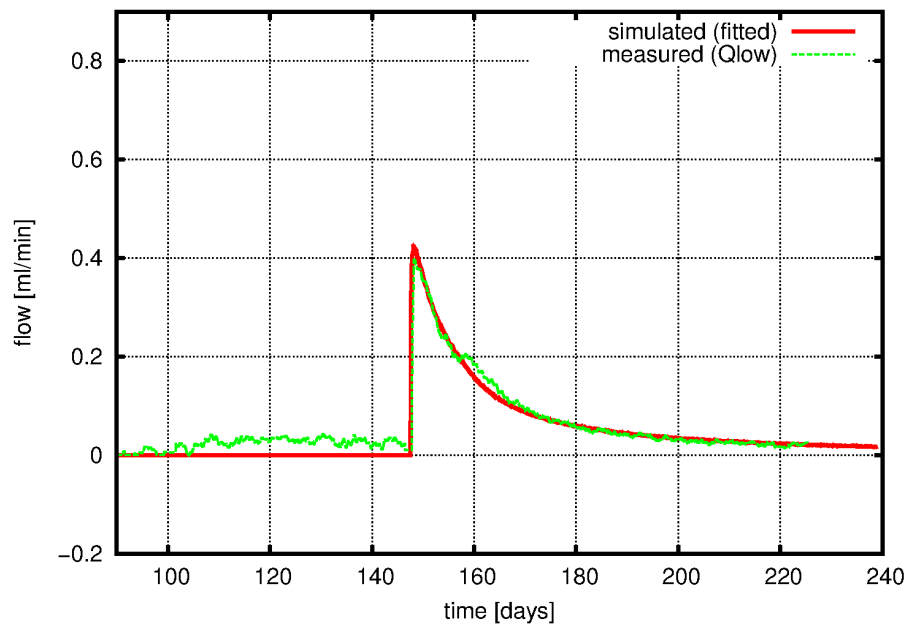
Fig. 4.6   Gas flows of the best-fit calculation together with the measured flows

Fig. 4.7 shows the evolution of the secondary porosity at nine different grid elements. The lengths displayed in the key of Fig. 4.7 denote the distances between the centre of the respective grid element and the border of the injection interval. All element centres are placed on a line which is aligned normal to the borehole axis and runs through the centre of the injection interval.

According to Fig. 4.7, dilation was detected 135 cm away from the injection borehole but there was no sign of dilation at a distance of 150 cm. At distances beyond 114 cm, the rate of porosity change decreased to zero already after a few days. Therefore, the active dilation zone had a width of about 1 m.

At the beginning of pressure step HI5 all points started to dilate at the same time, which means that the dilation zone already reached its final width shortly after the first pressure pulse of HI5. The different rates of porosity change were caused by the general pressure decrease with increasing distance.
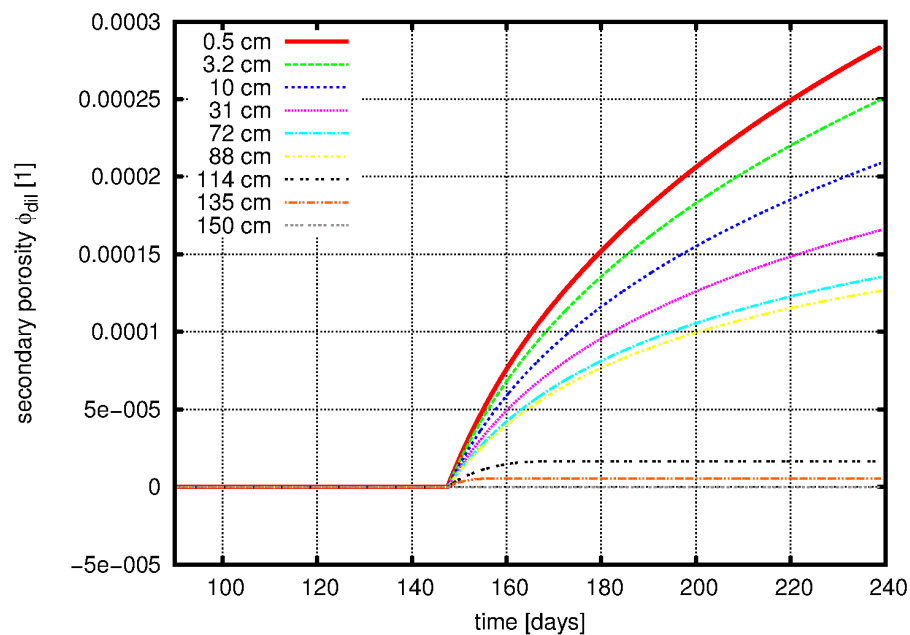
Fig. 4.7   Secondary porosity at different distances from the border of the injection interval

The reduction of the threshold pressure is displayed in Fig. 4.8 for five different grid elements. The initial threshold pressure is 2.35 MPa. Triggered by the pressure pulse of step HI5 there are softening reactions in the entire dilation zone. For distances up to 88 cm the threshold pressure drops to the minimum value prescribed by parameter

$p_{\text{thr}}^{\min}$ (1.1 MPa). At distances of 114 cm, 135cm, and 150 cm there is less softening because the pressure does not reach p_{soft} .
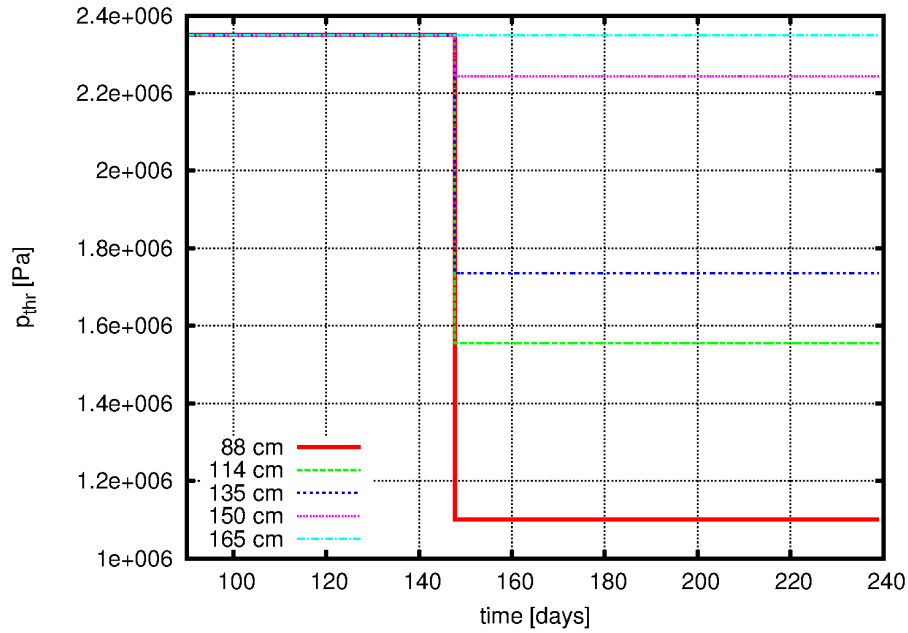
Fig. 4.8   Threshold pressures at different distances from the border of the injection interval

The pressure evolution is plotted in Fig. 4.9 for ten different grid elements. Before step HI5, all elements were at the initial pressure of 2.34 MPa. At the time of the HI5 pressure pulse, all grid elements dilated simultaneously. However, each grid element experienced a different pressure at this time, which reflected the prevailing pressure gradient. The pressure gradient at the beginning of pressure step HI5 therefore controlled the extent of the dilation zone.

After gas entry, pressures decreased due to the expansion of the gas phase caused by the given dilation rates. Pressures reached the threshold pressure at distances of 114 cm, 135 cm, and 150 cm (Fig. 4.9) and remained constant afterwards because of the vanishing permeability. This means that the gas phase was shut-in at the threshold pressure.
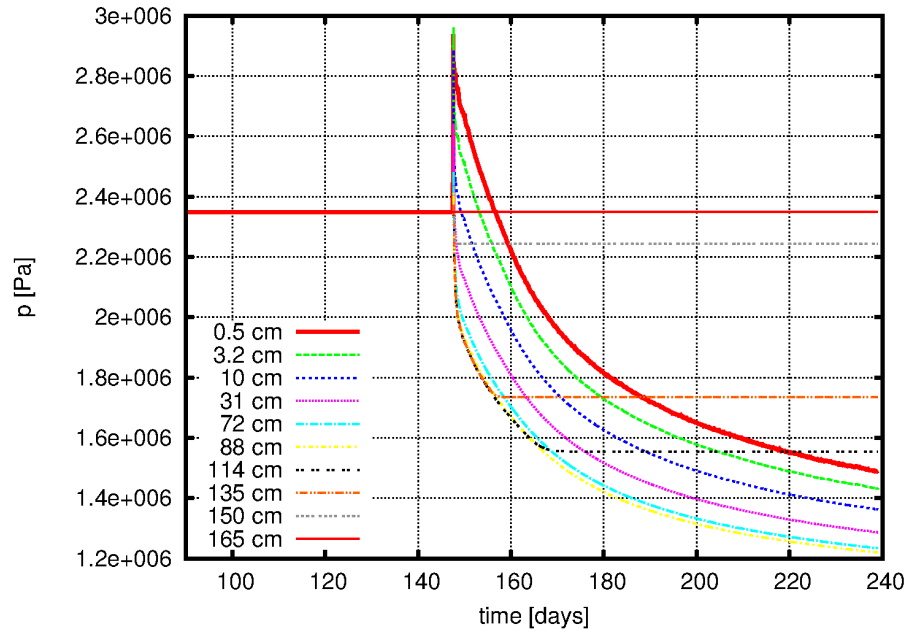
Fig. 4.9　　Pressures at different distances from the border of the injection interval

4.3.4　　　　Parameter variation

The sensitivity of the model was investigated by varying single parameters against the fitted values. To appraise the effect of such variations it has to be remembered that the injection pressure was defined as a pressure boundary condition, while in the real system it is coupled to the injection flow. Due to the boundary condition, the model may produce vanishing or even negative injection flows while the injection pressure is decreasing. This could never be the case in the real system where every pressure decrease is a consequence of a positive gas flow into the rock (provided that there is no leakage from the experimental devices).

4.3.4.1   Varying the dilation rate

The dilation rate (the rate of porosity change) is controlled by the parameter C_2. As C_2 was increased there was also an increase of the gas flow, and vice versa (see Fig. 4.10). The change of gas flow was not proportional to the change of C_2.
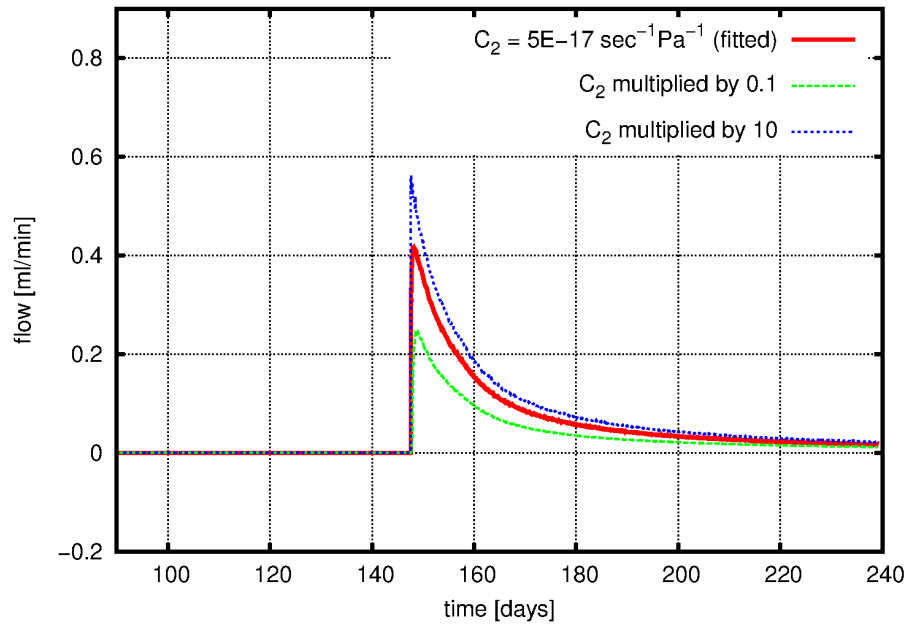
Fig. 4.10   Varying the dilation rate using parameter C_2

Interpretation

In the model, gas can only enter if the dilation rate is larger than zero. The parameter C_2, controlling the dilation rate directly via equation (4.2), therefore has an immediate effect on gas injection. However, the high value of C_2 (factor 10) probably caused a pressure decrease in the vicinity of the injection borehole. This reduced the width of the dilation zone to less than 72 cm (Fig. 4.11) and consequently reduced the uptake of gas. Therefore, gas injection was not proportional to C_2.
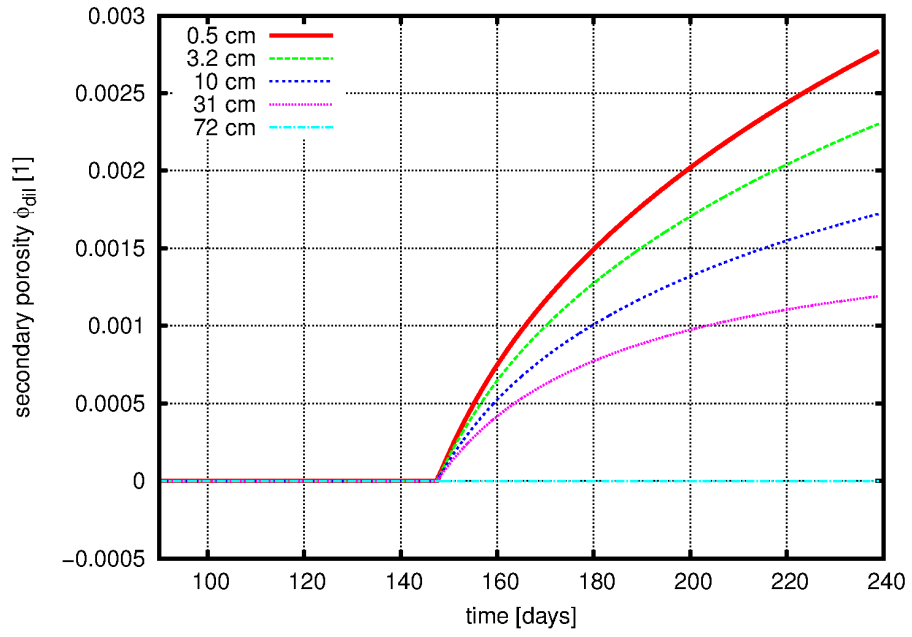
Fig. 4.11 Dilation rates if parameter C_2 is multiplied by a factor of 10

4.3.4.2 Varying the permeability of dilated elements

The permeability of dilated elements is controlled by the parameter C_1. Injection flows were significantly affected in step HI5 as C_1 was varied (see Fig. 4.12). The change of the injection flow was nearly proportional to the change of C_1.

Interpretation

Parameter C_1 controls how fast the pressure signal can travel from the injection interval into the rock. It therefore determines how many grid elements will manage to reach the threshold pressure for dilation. This again controls the width of the dilation zone, which explains why C_1 has such a strong influence on gas flow.
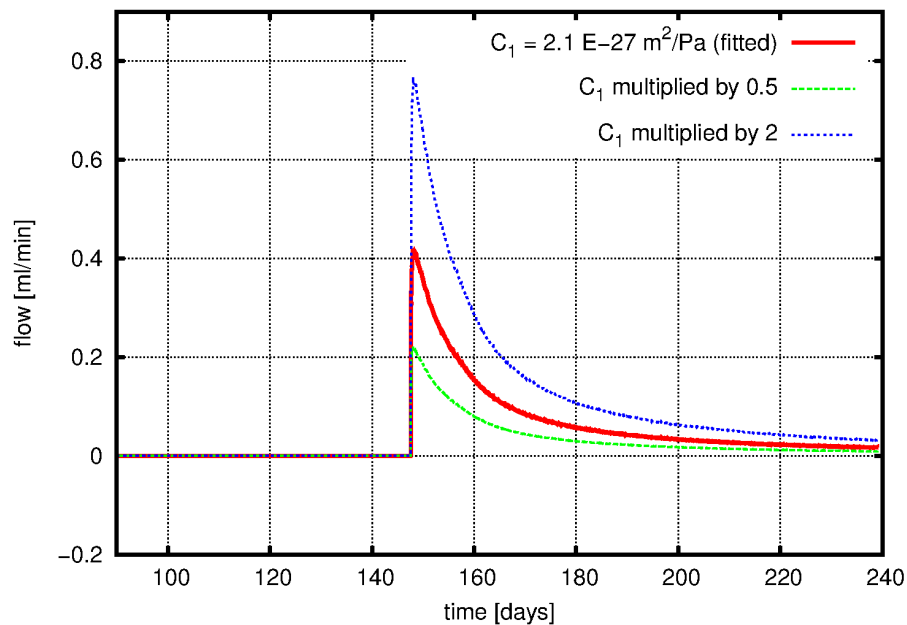
Fig. 4.12   Varying permeability using parameter C_1

4.3.4.3 Varying the initial threshold pressure

The initial threshold pressure was decreased to 2.3 MPa, 2.2 MPa, and 2.1 MPa. These values are below the maximum pressure of pressure step HI4 so that a gas flow already established itself in step HI4.

As Fig. 4.13 shows, the variation changed the shape of the flow curves. The same curves are obtained for initial thresholds of 2.2 MPa and 2.1 MPa. For these initial

thresholds, an elevated flow peak develops at the beginning of step HI5 and the injection flow decreases more quickly in the following days. The tendency towards a quicker decrease of gas flow is also visible in step HI4 (starting on day 100).

Interpretation

The decrease of gas flow that is visible in step HI4 for initial thresholds of 2.2 MPa and 2.1 MPa was not caused by a decreasing dilation rate. As Fig. 4.14 illustrates, the dilation rate remained almost constant during pressure step HI4. More likely, the noticed decrease of gas flow reflects the decreasing injection pressure.

The sharp flow peak at the very beginning of step HI5 (same calculation case) attributes to the fact that there was already dilated pore space existing. This pore space had been created in step HI4. The pressurisation of the additional pore space in step HI5 required a flow of gas, which was visible as a flow peak.

Using an initial threshold of 2.1 MPa there was a quicker decrease of the injection flows during step HI5. This can be explained by the fact that a reduced initial threshold allows the gas to enter the rock already at lower pressures, i. e. in pressure step HI4. This reduces the dilation-driven *relative* increase of the gas-filled porosity in pressure step HI5, which acts as a gas sink inside the rock by expanding the gas phase and lowering pore pressures. The effect of dilation on gas flow therefore also depends on the amount of gas that is already present inside the rock.
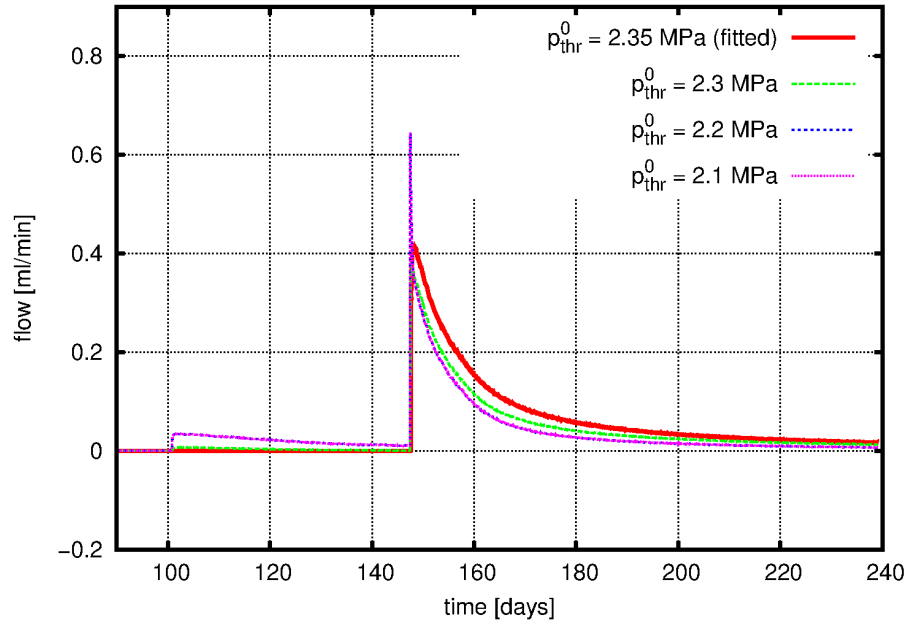
Fig. 4.13　Varying the initial pressure threshold p_{thr}^0 for pathway dilation
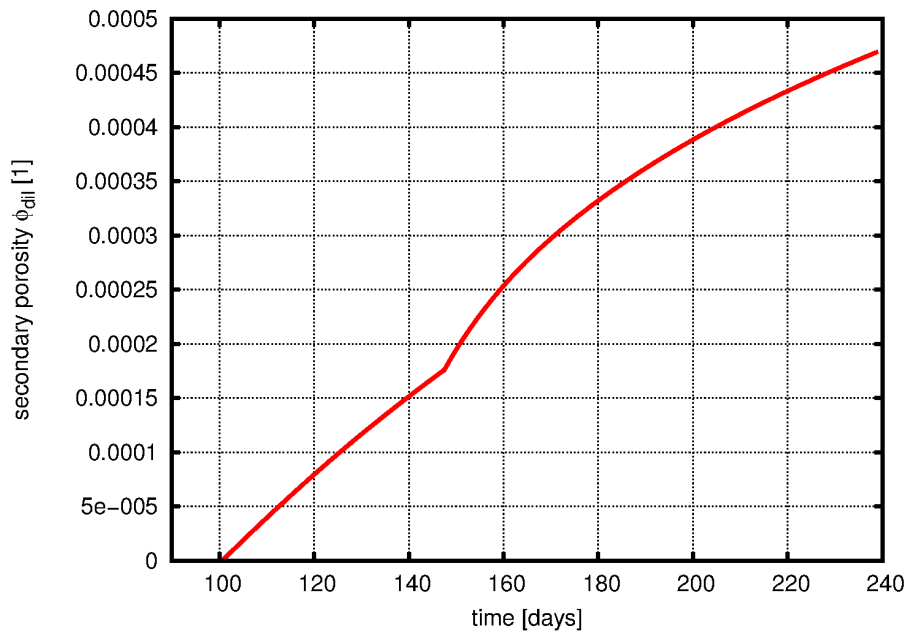
Fig. 4.14　Secondary porosity of the element nearest to the injection borehole for an initial threshold of 2.1 MPa

4.3.4.4   Varying the minimum threshold pressure

The degree of softening against microscopic tensile failure is determined by the parameter $p_{\text{thr}}^{\text{min}}$. The threshold pressure falls to the value of this parameter if the pressure reaches p_{soft}.

In the best-fit calculation $p_{\text{thr}}^{\text{min}}$ was set to 1.1 MPa. The effect of increasing and lowering this value can be studied in Fig. 4.15. For a value of 2.2 MPa the gas flow decreased and occurred only between day 147 and 160. The gas flow increased for a value of 0.55 MPa. Of all model parameters, parameter $p_{\text{thr}}^{\text{min}}$ is the one with the strongest long-term influence on gas flow.

Interpretation

As the minimum threshold pressure was raised to 2.2 MPa, the decreasing pore pressures arrived at the threshold pressure earlier. This stopped dilation, permeability vanished and the injection flow ceased. This process represents the closure of a certain part of the pore network, which is relevant for flow.
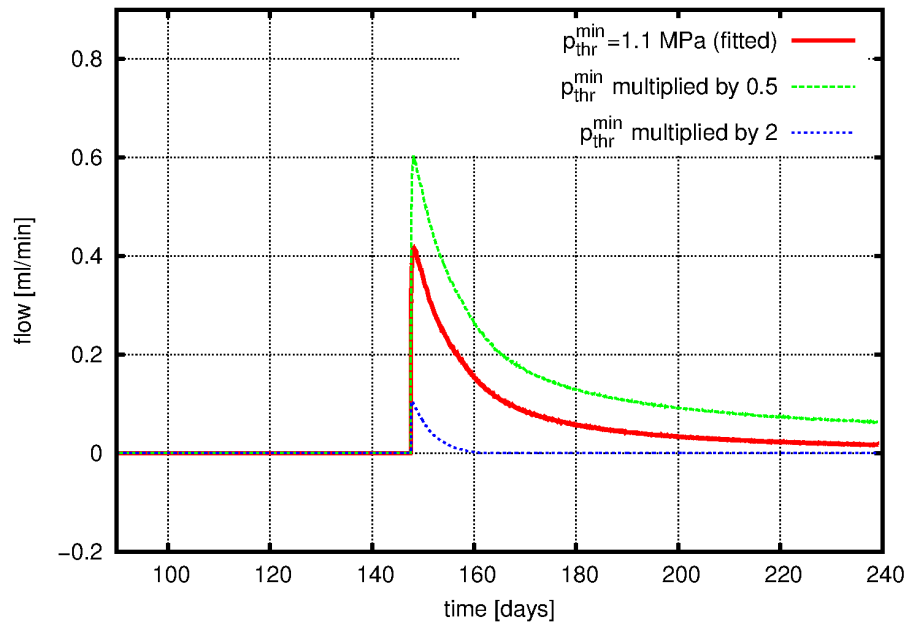
Fig. 4.15   Varying the residual pressure threshold $\boldsymbol{p}_{\text{thr}}^{\text{min}}$ for pathway dilation

4.3.4.5   Varying the softening pressure

The pore pressure for which the threshold pressure reaches its lowest possible value is determined by the parameter p_{soft}. In the analysis it was only possible to increase this parameter because the fitted value of p_{soft} (2.4 MPa) was already close above the initial threshold pressure of 2.35 MPa (p_{soft} always has to be larger than the threshold pressure). Fig. 4.16 shows how the injection flows changed as p_{soft} was set to 2.6 MPa and 2.8 MPa, respectively. The injection flows clearly decreased with increasing value of p_{soft}.

Interpretation

For an increased value of p_{soft}, distant points find it more difficult to raise the pore pressure to p_{soft} and thus to achieve full softening. Thresholds for dilation therefore remain higher so that dilation stops earlier. This reduces the injection flow.

The difficulty to reach full softening is highlighted by the threshold evolution for $p_{\text{soft}} = 2.8$ MPa (see Fig. 4.17). The rock failed to reach full softening ($p_{\text{thr}}^{\min}=1.1$ MPa) already 31 cm away from the injection borehole (114 cm for the fitted parameters).
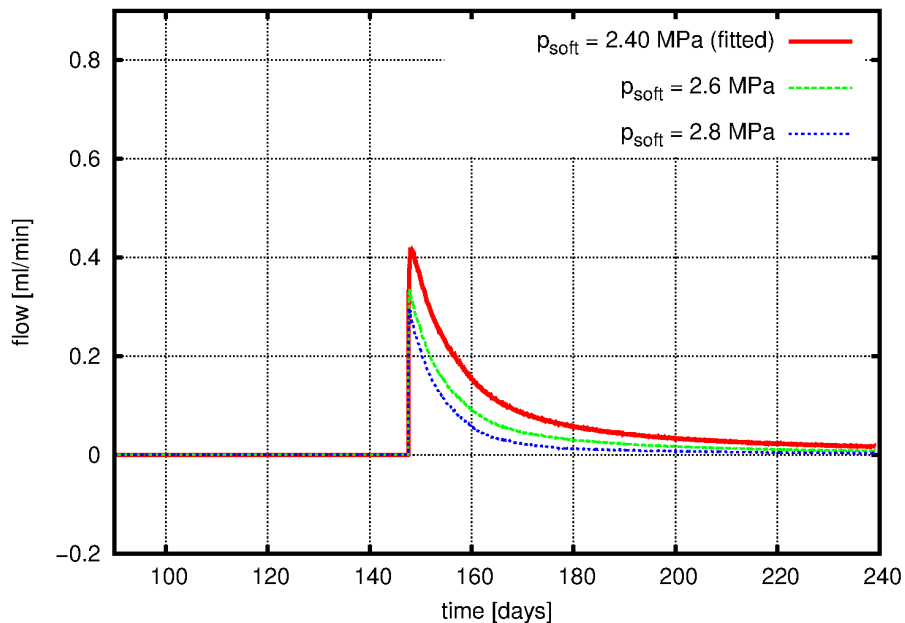
Fig. 4.16   Varying the pressure threshold p_{soft} for maximum softening
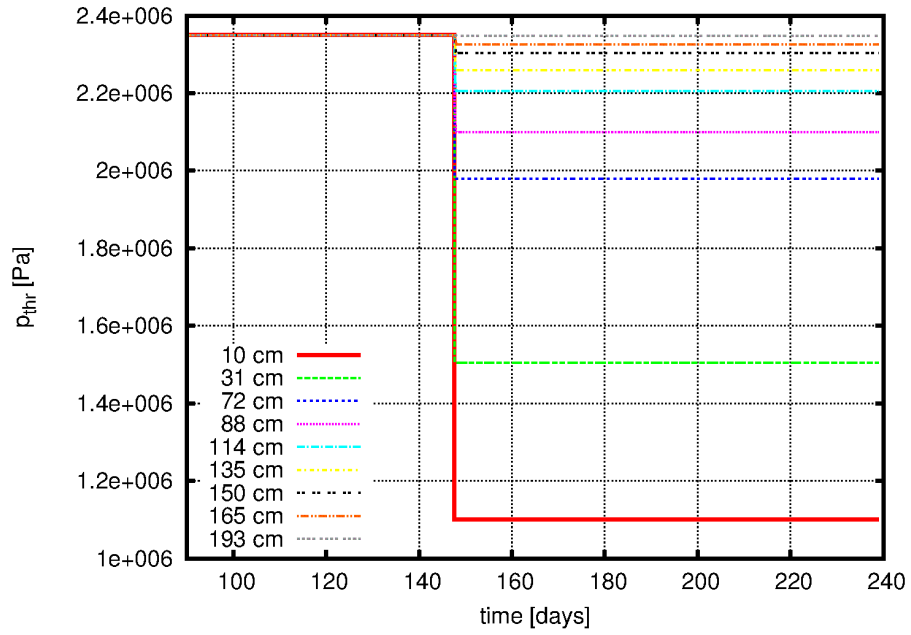
Fig. 4.17   Threshold pressure at different distances for $p_{\text{soft}} = 2.8$ MPa

4.3.4.6   Varying anisotropy

The anisotropy of permeability was varied by means of the tensor K_{dil}. Only the third component k_3 of the tensor was changed. This component is oriented perpendicular to bedding, i. e. parallel to the borehole axis.

Fig. 4.18 shows the effect of setting k_3 to 0 and 1. Apparently, anisotropy had no strong influence on gas flow.

Interpretation

An increase of k_3 increases the width of the dilation zone perpendicular to bedding. This change of width is probably small compared to the length of the injection interval. Changes in k_3 therefore only have a low impact on gas injection. This is a consequence of the experimental set-up.
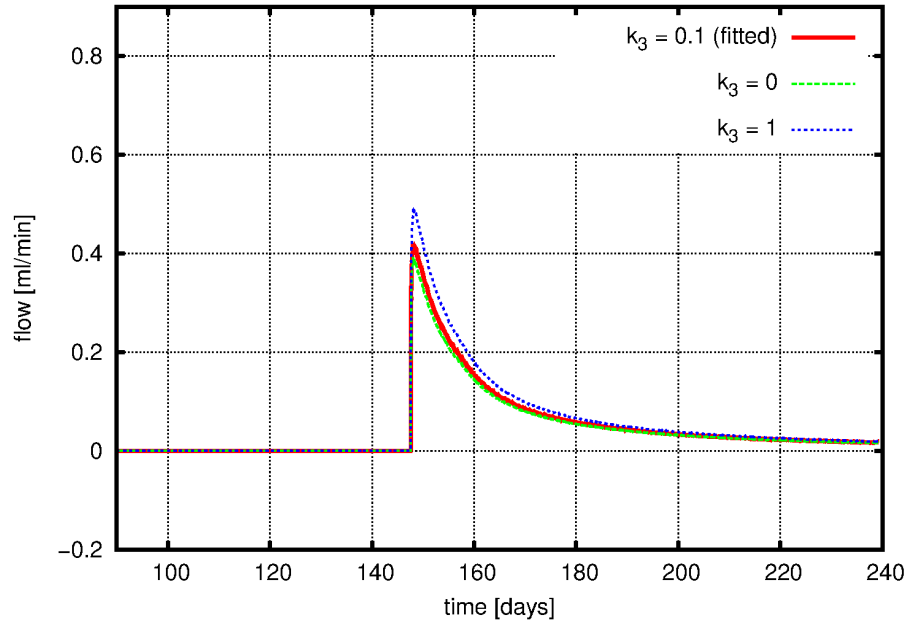
Fig. 4.18   Varying isotropy

4.3.5   Alternative parameter fit

It was possible to achieve a good curve fit with an alternative parameter set (see Tab. 4.2). The difference to the first fit (Tab. 4.1) is a higher value of C_2 (responsible for the dilation rate). The increased dilation rate is compensated by a lower value of C_1 (controlling the permeability). Fig. 4.19 shows the quality of this fit.

Tab. 4.2   Alternative parameter fit for the dilation model

C_1	1.6 E-27 m²/Pa
C_2	1 E-15 sec^{-1}Pa^{-1}
p_{thr}^0	2.35 MPa
p_{thr}^{min}	1.1 MPa
p_{soft}	2.4 MPa
K_{dil}	$(1, 1, k_3)$ with $k_3 = 0.1$
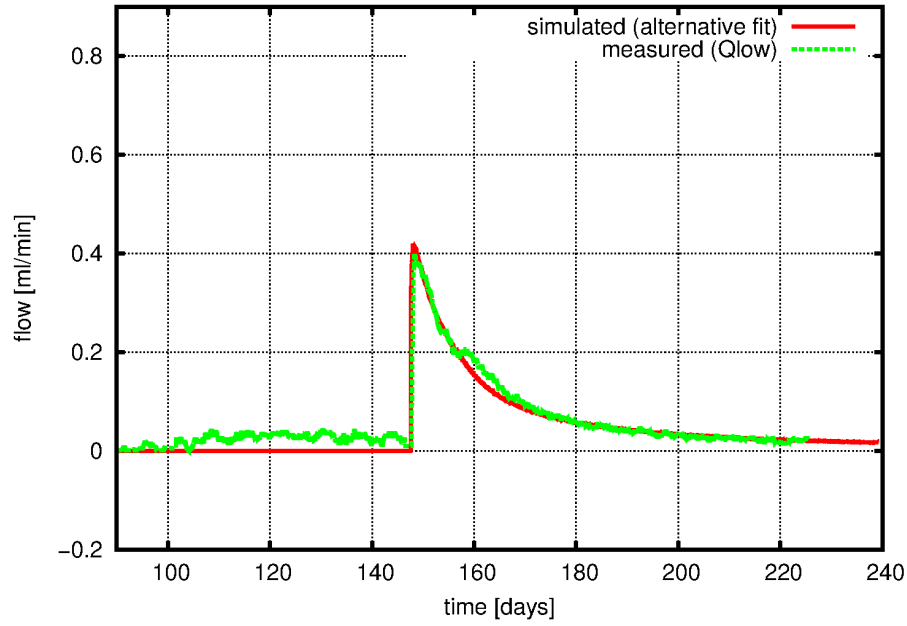
Fig. 4.19 Gas flows for the alternative set of fitted parameters

The two fitted parameter sets produced a different width of the dilation zone. Using the alternative parameters, pathway dilation was absent at a distance of 31 cm (Fig. 4.20). Thus, the dilation zone was much narrower. Calibrating the model only against the injection flow is apparently not sufficient to determine the model parameters uniquely.
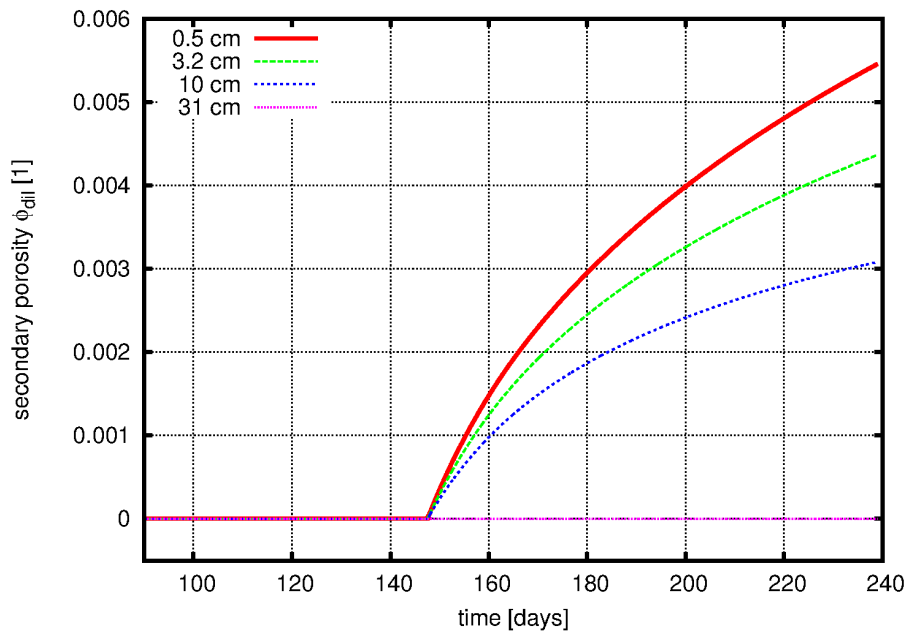
Fig. 4.20 Secondary porosity at different distances from the border of the injection interval (alternative parameter set)

53

4.4　　　Models with increased phase interaction

Two model variants were derived from the pathway dilation model in order to investigate the effects of processes that provide additional gas storage inside the rock. The "water compression model" was yielded by turning on water compression in the pathway dilation model. The "gas dissolution model" was derived from the pathway dilation model by turning on gas dissolution. Dissolving gas means that gas can be stored with increasing pressure and is again released with decreasing pressure. Both models assume that the interface between liquid and gas phase in the rock is large enough to produce considerable phase interactions like water compression or gas dissolution.

Fig. 4.21 shows the injection flows which were calculated by the water compression model. Obviously, the injection flows decreased faster.

The effect of gas dissolution can be seen in Fig. 4.22. Gas dissolution apparently had a strong effect on the injection flows. These decreased so fast that they even caused a backflow. The model allows a backflow only if the pressure remains above the threshold pressure (otherwise the permeability would be zero). These high pressures were probably caused by the outgassing of the liquid. This process finally inverted the pressure gradient and created the backflow.

Both simulations show that additional gas storage in the rock leads to a faster decrease of the injection flows. The results of the previous section suggest that no parameter of the pathway dilation model would be able to compensate the fast decrease of injection flows in order to fit the measured data. This leads to the conclusion that gas dissolution and water compression do not play a major role in the system, which probably attributes to a small interface area between water and gas. This again might be caused by a high localisation of dilating gas pathways.
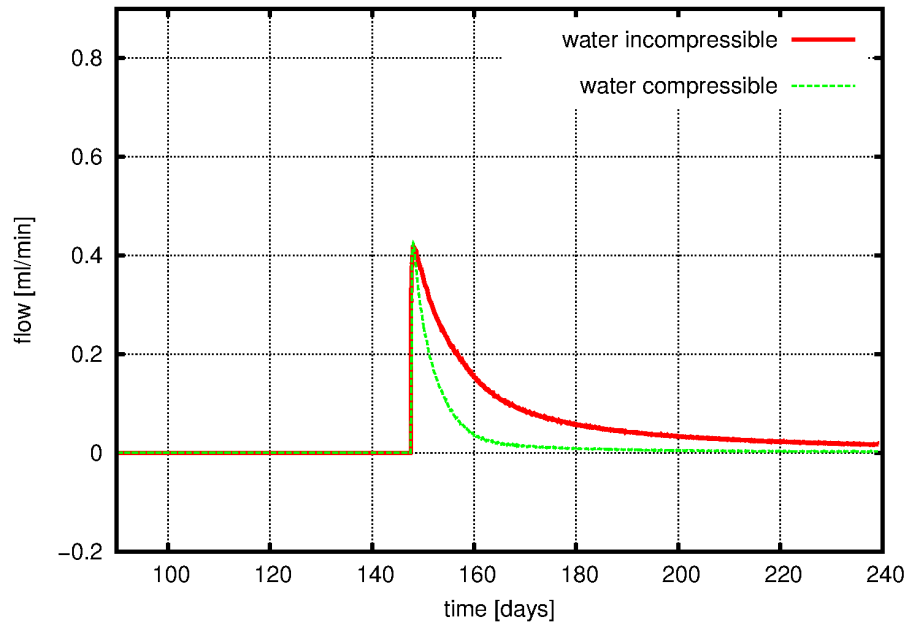
Fig. 4.21   Injection flows with and without water compression
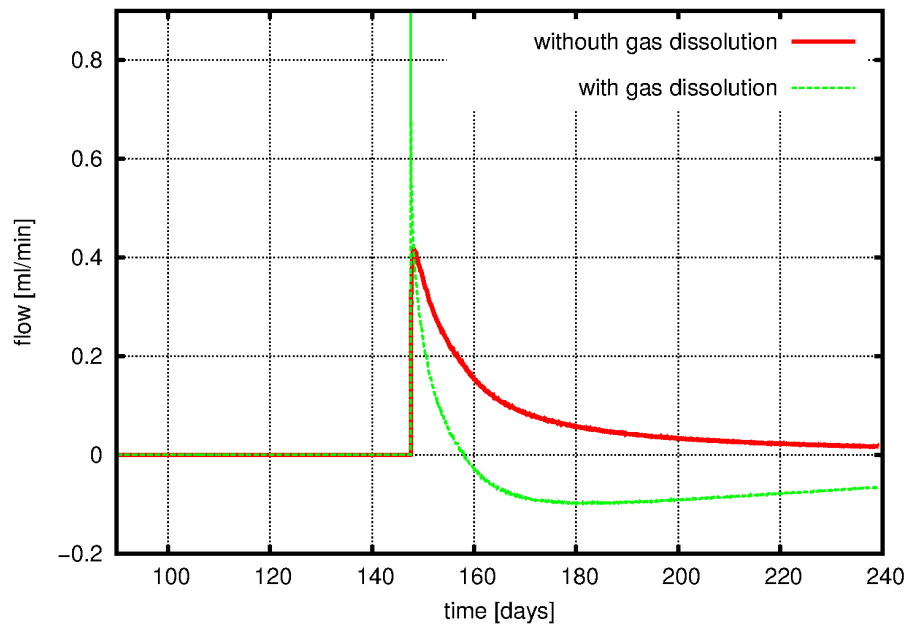
Fig. 4.22   Injection flows with and without gas dissolution

4.5　　Tube-chamber model 1

In the pathway dilation model described before, a pressure-dependent injection flow was created by introducing a pressure-dependent dilation rate of the rock. However, other ways of introducing a pressure-dependent injection flow should be possible. For example, a similar behaviour could be achieved by using a remote air-filled chamber which is charged with gas by the injection interval. The magnitude of the injection flow would then depend on the pressure difference between chamber and injection interval. These considerations provided the impulse for the development of the tube-chamber model, which is described in the following.

4.5.1　　Model description

The tube-chamber model is a simple representation of a preferential pathway that runs from the injection interval to a remote air filled chamber. The connection between both is established by a tube, which contains a porous medium. The remote chamber may be a borehole or a drained part of the rock or of a fracture. Fig. 4.23 shows the principal set-up. There is no liquid in the entire system. If the gas pressure inside the injection interval exceeds that of the chamber, gas is pressed through the tube and into the chamber. Consequently, the chamber pressure increases.

A pressure, density, and viscosity gradient will evolve along the tube if there is a pressure difference between the injection interval and the chamber. In order to simplify the description of the system it was assumed that the flow of gas through the tube can be described by Darcy's law using an effective pressure gradient, density and viscosity. If p_1 is the pressure of the injection interval, p_2 the chamber pressure and x the length of the tube, the effective pressure gradient shall be

$$\frac{p_1 - p_2}{x}.$$

The effective gas density inside the tube was assumed to be the density of an ideal gas at the mean pressure:

$$\rho_{\text{eff}} = \frac{p_1 + p_2}{2} \frac{M}{RT}.$$

With this approximation and by introducing effective values also for the permeability and viscosity, Darcy's law for the mass flow of gas through the tube takes the form

$$Q = \frac{k_{\text{eff}}(p, p_{\text{thr}}) A \rho_{\text{eff}}}{\mu_{\text{eff}}} \cdot \frac{p_1 - p_2}{x}.$$

Here, k_{eff} is the pressure-dependent permeability of the porous medium in the tube, A is the cross-sectional area of the tube, μ_{eff} the effective dynamic viscosity of gas, and x the distance between injection interval and chamber.

A pressure threshold p_{thr}^i for gas flow was introduced in analogy to the pathway dilation model. p_{thr}^i is the threshold pressure at time step i with $i = 0$ at the beginning of the simulation. The effective permeability k_{eff} of the porous medium was defined by

$$k_{\text{eff}} = (p_1 - p_{\text{thr}}^i) C_1 \quad \text{for} \quad p_1 \geq p_{\text{thr}}^i \quad \text{and} \quad k_{\text{eff}} = 0 \quad \text{for} \quad p_1 < p_{\text{thr}}^i.$$

Using this definition and substituting ρ_{eff}, the equation for mass flow reads

$$Q = (p_1 - p_{\text{thr}}^i)(p_1{}^2 - p_2{}^2) \frac{C_1 A M}{2 \mu_{\text{eff}} x RT} \quad \text{for} \quad p_1 \geq p_{\text{thr}}^i$$

with $Q = 0$ for $p_1 < p_{\text{thr}}^i$. The *volumetric* flow for $p_1 \geq p_{\text{thr}}^i$ at reference pressure p_{ref} and reference temperature T_{ref} can now be calculated by

$$Q_{\text{vol}} = Q \frac{RT_{\text{ref}}}{M p_{\text{ref}}} = (p_1 - p_{\text{thr}}^i)(p_1{}^2 - p_2{}^2) \frac{C_1 A T_{\text{ref}}}{2 \mu_{\text{eff}} x T p_{\text{ref}}}$$

With the fitting parameter

$$c = \frac{C_1 A T_{\text{ref}}}{2 \mu_{\text{eff}} x T p_{\text{ref}}}$$

the formulation of the volumetric flow simplifies to

$$Q_{\text{vol}} = (p_1 - p_{\text{thr}}^i)(p_1{}^2 - p_2{}^2) c.$$

A pressure-dependent softening of the porous medium was described to occur by reducing the threshold pressure with increasing interval pressure. A pressure $\hat{p}_{thr}$ was introduced in order to calculate the threshold pressure p_{thr}^i. $\hat{p}_{thr}$ is the reduced threshold pressure that would develop in undisturbed rock by applying the injection pressure p_1:

$$\hat{p}_{thr} = \frac{p_1 - p_{thr}^0}{p_{soft} - p_{thr}^0}\left(p_{thr}^{min} - p_{thr}^0\right) + p_{thr}^0 \quad \text{for} \quad p_{soft} \geq p_1 \geq p_{thr}^0$$

$$\hat{p}_{thr} = p_{thr}^{min} \quad \text{for} \quad p_1 > p_{soft}$$

$$\hat{p}_{thr} = p_{thr}^0 \quad \text{for} \quad p_1 < p_{thr}^0 .$$

Softening was then introdruced by

$$p_{thr}^i = \min\left(p_{thr}^{i-1}, \hat{p}_{thr}\right).$$

By setting the mass flux equal to the mass increase inside the chamber, the rate of pressure change inside the chamber was calculated using the ideal gas law:

$$\frac{dp_2}{dt} = Q_{vol}\frac{T\,p_{ref}}{T_{ref}V}.$$

Here, V is the volume of the chamber. The initial condition is $p_2(t = 0) = p_{2,ini}$.
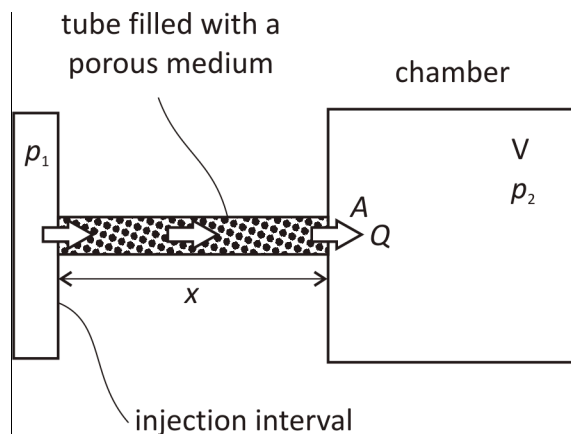
Fig. 4.23 Sketch of the tube-chamber model

4.5.2 Results

The calibration of the tube-chamber model against the measured flow data yielded the parameter values listed in Tab. 4.3.

Tab. 4.3   Fitted Parameters for the tube-chamber model

c	5.0E-28 m^3 s^{-1} Pa^{-3}
$p_{2,ini}$	0.7 MPa
p_{thr}^0	2.35 MPa
p_{thr}^{min}	1.1 MPa
p_{soft}	2.4 MPa
V	0.004 m³ = 4 l (good fits achievable for V > 4 l)
T	21 °C
T_{ref}	21 °C
p_{ref}	0.1 MPa

The simulated and measured flows are displayed in Fig. 4.24. There is a good agreement between both curves. The chosen chamber volume was relatively large, which is the reason why the chamber pressure only rose to approx. 1 MPa (Fig. 4.25). It was found that V = 4 litres was a lower limit for which good fits could be achieved (see Fig. 4.24). Above V = 4 l the flow curve were not sensible against the parameter V.
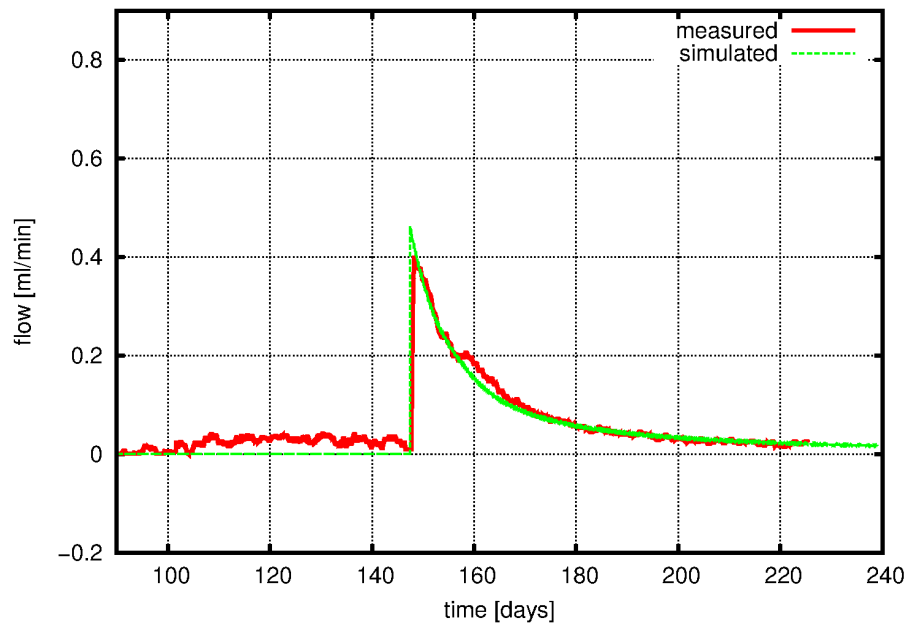
Fig. 4.24   Measured and simulated flows (tube-chamber model 1)
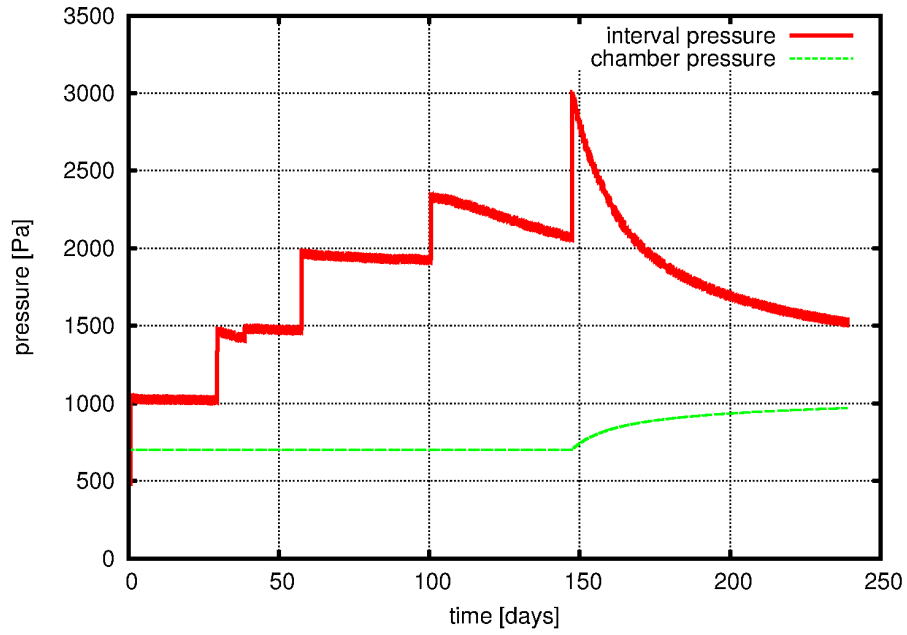
Fig. 4.25 Interval pressure (boundary condition) and simulated chamber pressure (tube-chamber model 1)
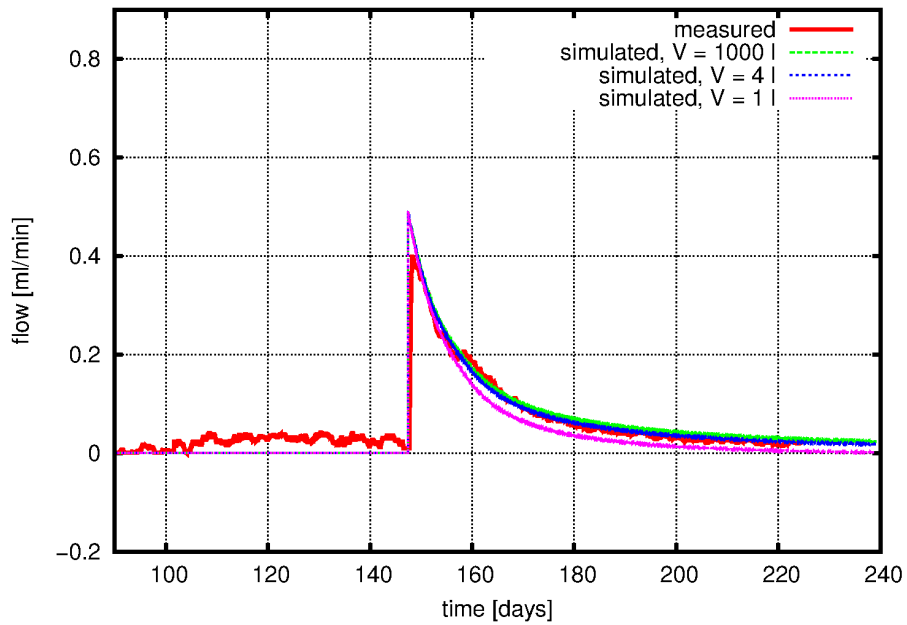
Fig. 4.26 Measured and simulated flows using different chamber volumes (tube-chamber model 1)

4.6 Chapter summary

Five models were applied to phase 2 of the HG-C experiment:

- The **variable permeability model** with pressure-dependent permeability,

- the **pathway dilaton model** with pressure-dependent dilation rate, dilation threshold, softening and minor phase interaction (absence of water compression and gas dissolution),

- the **water compression model**, which is the pathway dilation model with activated water compression,

- the **gas dissolution model**, which is the pathway dilation model with activated gas dissolution, and

- **tube-chamber model 1** with flow threshold and softening.

The variable permeability model and the water compression and gas dissolution models were unable to reproduce the measured injection flows. Good fits were achieved with the pathway dilation model and with tube-chamber model 1.

Findings for the pathway dilation model

- At the beginning of pressure step HI5, the dilation zone grew quickly to its final width. The width of the dilation zone was controlled by the pressure gradient in the clay. As soon as the pressure threshold was locally exceeded, the threshold was reduced (softening against microscopic tensile failure) and dilation commenced with a pressure-dependent dilation rate. The gas phase expanded and the pressure decreased. As soon as the decreasing pressures reached the threshold pressure, dilation stopped and the gas phase was shut-in at the threshold pressure.

- The model allowed a good fit of the gas flow measurements for pressure step HI5. However, different parameter sets which produced different widths of the dilation zone were able to deliver good fits. This implies that the flow data itself is not sufficient to determine the geometry of the dilation zone uniquely.

- The permeability of the dilated pores has a strong influence on the rate of gas injection and the width of the dilation zone.

- The dilation rate has a minor influence on the rate of gas injection because the width of the dilation zone decreases with increasing dilation rate.

- In the long term, injection flows are mostly influenced by the maximum degree of softening, which is expressed by the minimal threshold pressure.

- Although gradual softening was introduced by parameter p_{soft}, immediate softening (p_{soft} closely above p_{thr}^0) was used in all parameter fits and yielded satisfying results. Omitting p_{soft} would therefore be a possibility to simplify the model even further.

- Varying the permeability perpendicular to bedding did not have a major effect on gas flow. This probably attributes to the large length of the injection interval.

Findings for tube-chamber model 1

- The model assumes a drained cavity that is connected to the injection interval. At the experimental site, such a cavity could be an existing borehole or a part of the given hydro frac that has been drained by previous gas tests. It was estimated that the volume of this hypothetic cavity is not smaller than 4 litres.

5   HG-D Phase 2 (gas injection)

5.1   Experimental data and interpretation

The following data was provided for the gas injection phase of the HG-D experiment by Nagra:

- Pressures for all three intervals of boreholes BGS1, BGS2, and HGD in kPa.

- FIM measurements for boreholes BGS3 and BGS4.

- Injection flow rates in nml/min. As the flow measurements were too noisy, the gas flow into the rock (not the flow into the injection interval) was deduced from the decrease of the total gas volume inside the injection system and the pressure measurements by Solexperts.

- Two time series were provided for the injection flow. The first time series was calculated from the pressure of the pressure vessel, the second one from the pressure of the injection interval (interval 2 of borehole HGD). The flow data derived from the pressure in the injection interval represents the main flow data.

The provided data are plotted in Fig. 5.1 to Fig. 5.6. A time window of 162 days was chosen for all plots. This corresponds to the time window for which flow data were available. Time zero refers to the beginning of 29th October 2010 (midnight).

The two time series for gas flow are displayed in Fig. 5.1. Apparently, there is a good match between the flows that were calculated from the pressure of the pressure vessel and from the pressure of the injection interval (HGDi2), respectively. The latter flow data was used for the analysis.

Injection pressures and injection flows are displayed in Fig. 5.2. Compared to the gas injection phase of HG-C (Fig. 4.4, p. 35), higher flows were achieved in HG-D although the injection pressures were generally lower.

Further on, there is no obvious gas entry pressure in phase 2 of HG-D. In contrast, flow thresholds were present in all simulations that reproduced the gas injection phase of HG-C. It is not clear whether the missing flow threshold in HG-D is an artefact. However, the two experiments are substantially different and a blind prediction of phase 2 of

HG-D is apparently not possible with the models and parameter sets that were used for phase 2 of HG-C.
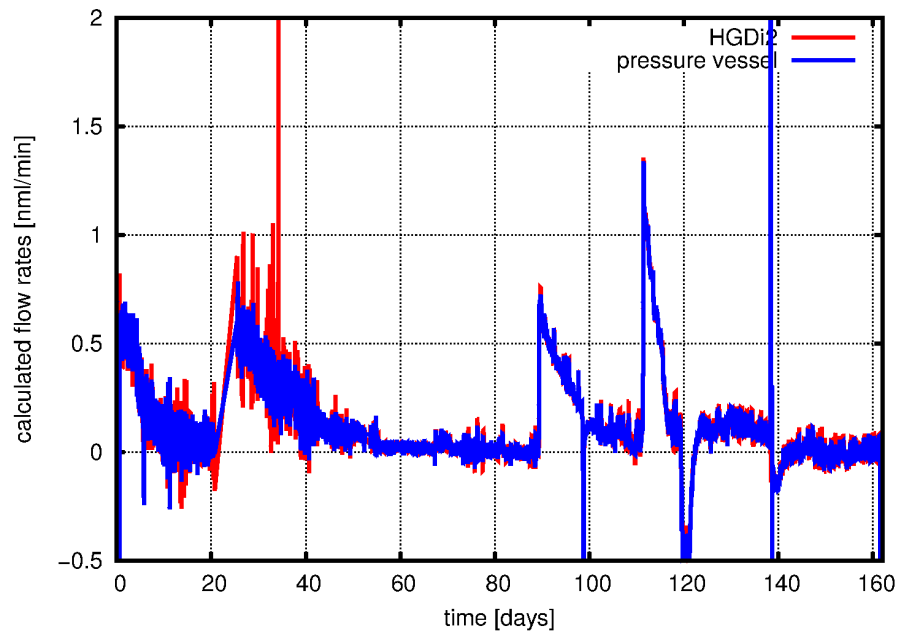
Fig. 5.1   Flow rates during gas injection (HG-D experiment)
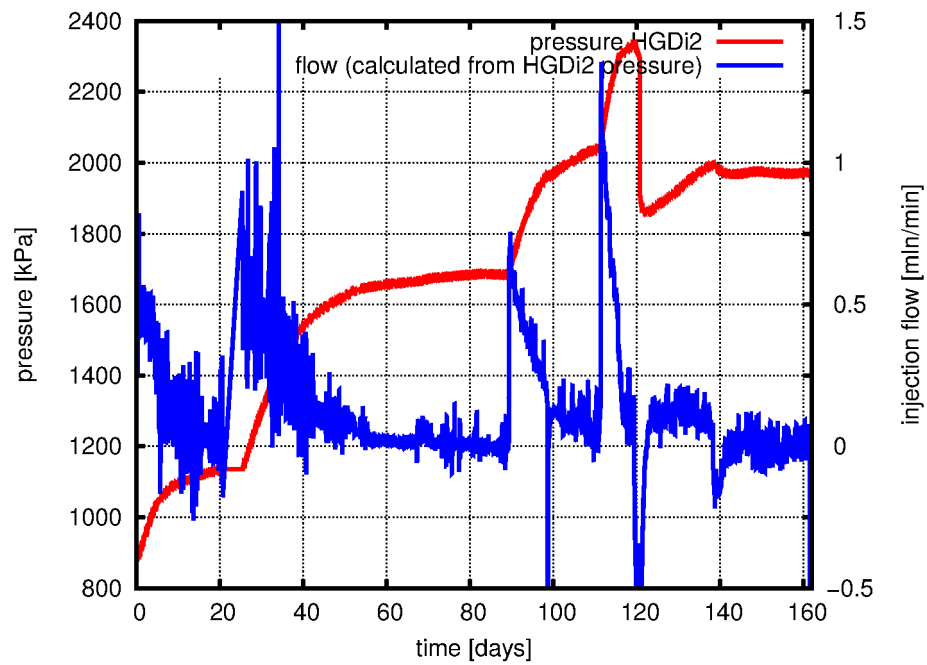
Fig. 5.2   Pressure in the injection interval and injection flow

Despite the lack of flow thresholds, interval 1 of borehole BGS1 showed a distinct pressure reaction on day 116 and thus a threshold-driven transport (Fig. 5.3). The reaction appeared during the fourth pressure step as the injection pressure was raised to 2300 kPa (Fig. 5.4). Interval 1 of BGS 1 also responded a second time on day 139 after a second pressure cycle. At that time the injection interval was pressurised with 2000 kPa.

Intervals 1 and 3 of borehole HGD showed a very slight response after day 120, which was too weak to be analysed (Fig. 5.5).
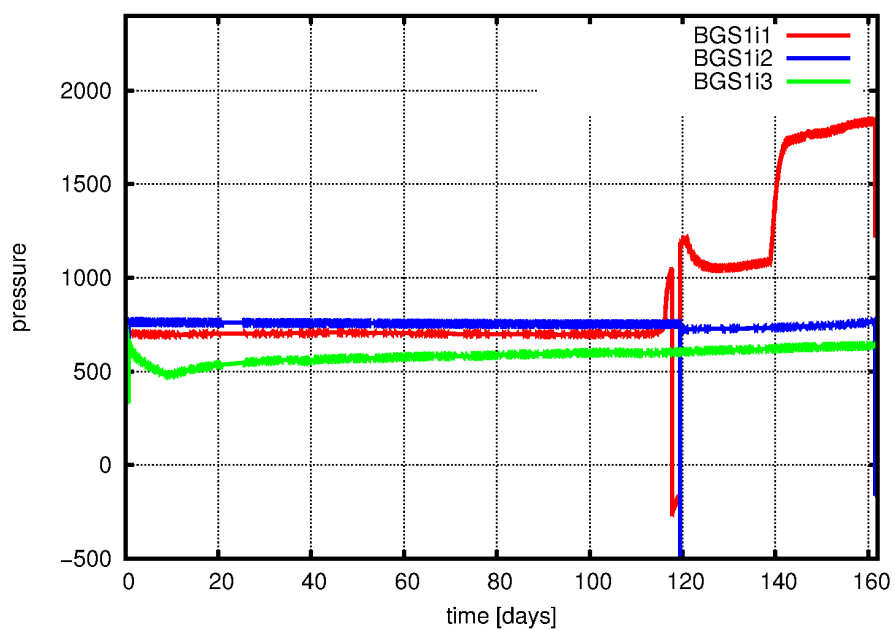
Fig. 5.3   Pressures measured in interval 1, 2, and 3 of borehole BGS1
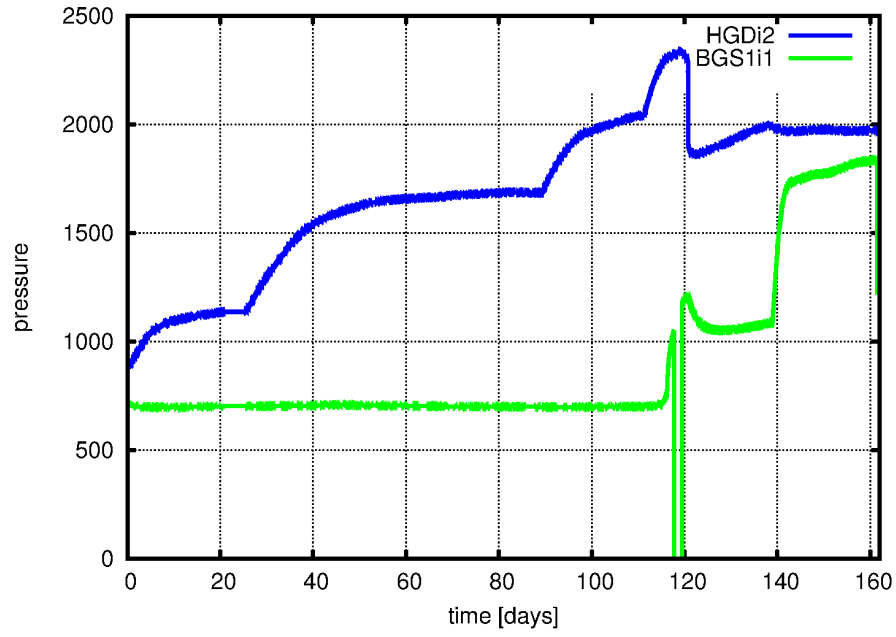
Fig. 5.4   Injection pressure and pressure in interval 1 of borehole BGS1
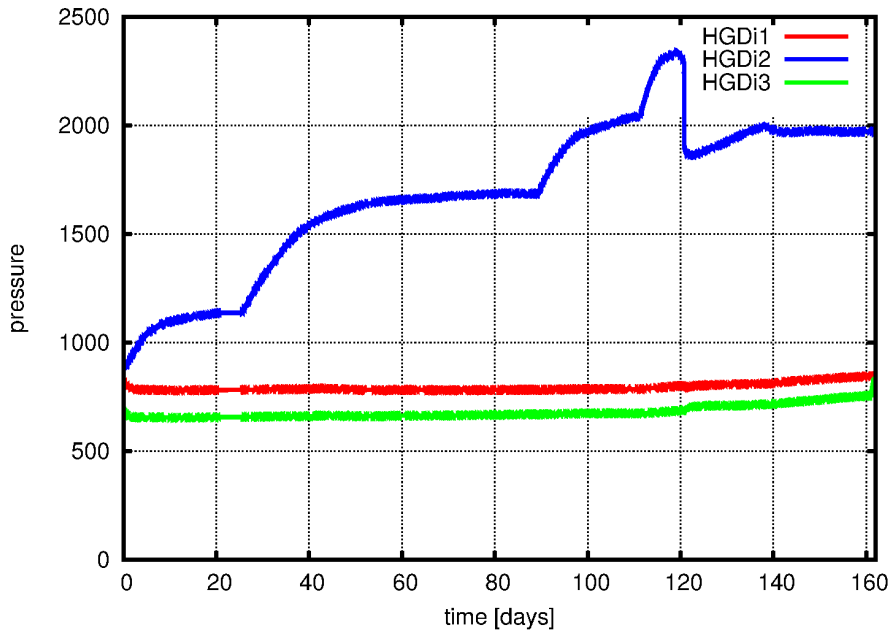
Fig. 5.5   Pressures in borehole HGD

66

The pressure measurements in interval 1 of borehole BGS2 were erroneous. The other intervals, 2 and 3, showed a general pressure increase (Fig. 5.6). There was a distinct pressure increase after day 143, which corresponds to the time of the second pressure reaction observed in interval 1 of borehole BGS1.
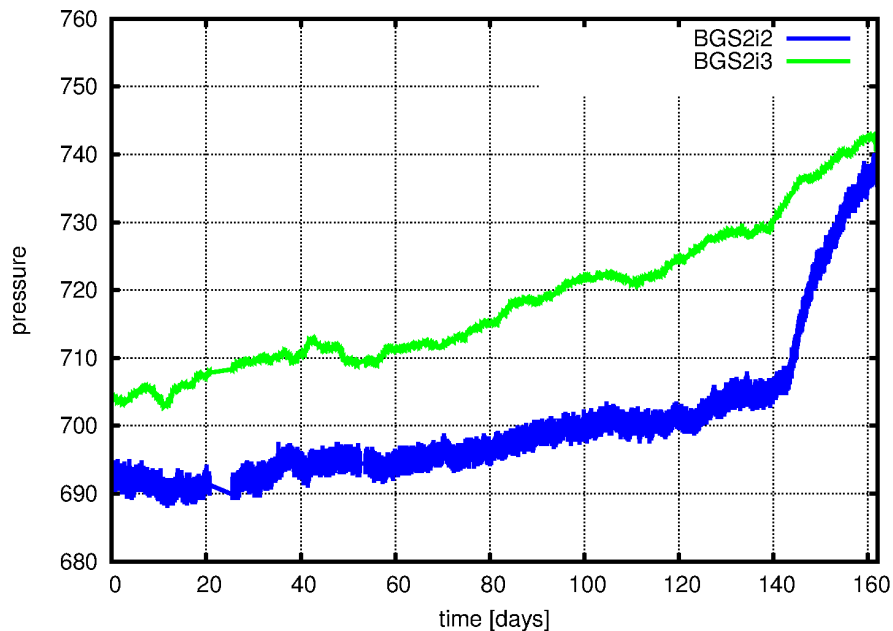
Fig. 5.6   Pressure evolution in interval 2 and 3 of borehole BGS2

Interval 3 of borehole BGS3 gave erroneous FIM data. The other intervals did not show any significant reaction compared to the amplitude of the signal's noise.

The FIM in interval 1 of borehole BGS4 gave erroneous values after about 120 days. The FIM measurements of intervals 3 and 2 showed a general linear trend which was difficult to correlate to any of the prescribed pressure steps.

5.2   Tube-chamber model 2

5.2.1   Model description

A second tube-chamber model ("tube-chamber model 2") was derived from tube-chamber model 1 in order to simulate phase 2 of the HG-D experiment. In this model, the permeability of the tube is constant.

We used the same formulation for the effective pressure and effective gas density as in tube-chamber model 1 and introduced effective values also for the permeability and viscosity. Herewith, Darcy's law for the mass flow of gas through the chamber was calculated by

$$Q = \frac{kA\rho_{\text{eff}}}{\mu_{\text{eff}}} \cdot \frac{p_1 - p_2}{x} = \frac{kAM}{2\mu_{\text{eff}}xRT} \cdot (p_1{}^2 - p_2{}^2).$$

In this equation, k is a constant permeability of the porous medium inside the tube. The volumetric flow at reference pressure p_{ref} and reference temperature T_{ref} was calculated by

$$Q_{\text{vol}} = Q \frac{RT_{\text{ref}}}{Mp_{\text{ref}}} = \frac{kA\,T_{\text{ref}}}{2\,\mu_{\text{eff}}\,x\,Tp_{\text{ref}}}(p_1{}^2 - p_2{}^2)$$

Gas flow leads to a pressure change inside the chamber which can be determined using the ideal gas law:

$$dp_2 = \frac{RT}{MV}dm = \frac{RT}{MV}Qdt$$

with $p_2(t = 0) = p_{2,\text{ini}}$ as initial condition. This leads to

$$\frac{dp_2}{dt} = \frac{kA}{2\mu_{\text{eff}}xV} \cdot (p_1{}^2 - p_2{}^2).$$

By introducing the fitting parameter

$$d = \frac{kA}{2\mu_{\text{eff}}x}$$

the equations for volumetric flow and pressure change simplify to

$$Q_{\text{vol}} = \frac{d\,T_{\text{ref}}}{Tp_{\text{ref}}}(p_1{}^2 - p_2{}^2) \qquad \text{and} \qquad \frac{dp_2}{dt} = \frac{d}{V} \cdot (p_1{}^2 - p_2{}^2).$$

5.2.2   Results

The calibration of tube-chamber model 2 yielded the parameter values listed in Tab. 5.1.

Tab. 5.1   Fitted parameters for tube-chamber model 2

d	6.0E-14 $m^3\ s^{-1}\ Pa^{-1}$
V	0.002 m³ = 2 l
T	21 °C
T_{ref}	21 °C
p_{ref}	0.1 MPa

The flow values simulated with these parameters are displayed in Fig. 5.7 together with the measured flows. There was remarkable agreement between both curves, indicating that the assumption of a missing flow threshold was correct. The high frequencies were reproduced very well, too. However, this may be an artificial effect because the experimental flow data have been calculated from the injection pressure. Therefore, the noise of the pressure signal was probably superimposed on the flow curve.

The lacking flow threshold points out that the injection interval has had a hydraulic connection to an undrained cavity, which might have been a part of the rock or of the experimental devices. It is therefore not sure whether the flow data are of artificial nature.

The characteristics of the rock are probably better reflected by the pressure measurements of borehole BGS1. The pressure reactions which have been observed here (see Fig. 5.4, p. 66) indicate that gas has percolated through the rock mass between the boreholes HGD and BGS1, and that this percolation was governed by a flow threshold.
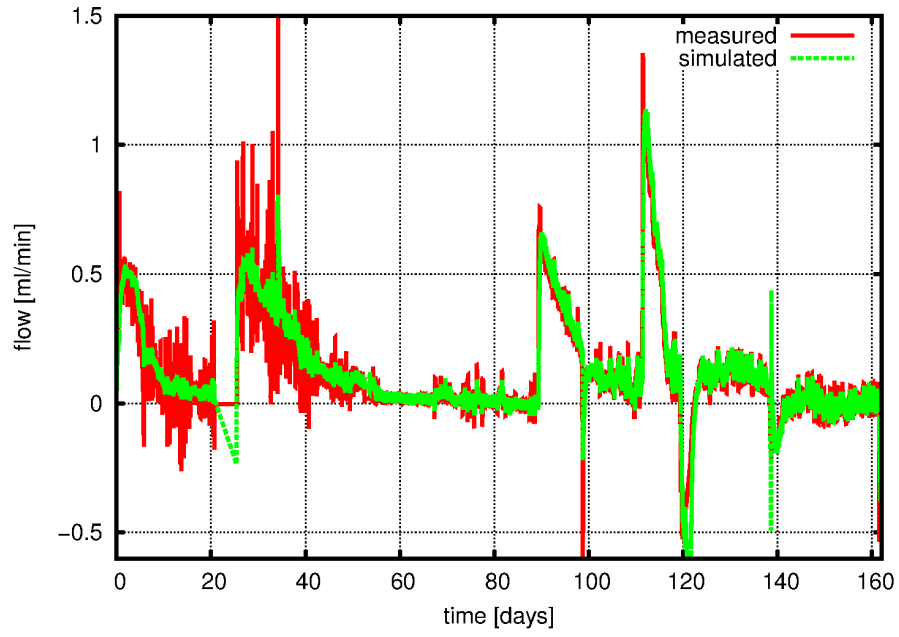
Fig. 5.7   Measured and simulated flows for the gas injection phase of the HG-D experiment

6   Discussion

The main goal of this study was to simulate the HG-C and HG-D experiments, which have been carried out at the Mont Terri Rock Laboratory, and to improve the understanding of gas migration in disturbed and undisturbed clay rocks. Another aim was to point out the limitations of typical performance assessment approaches as, for instance, two-phase flow and homogenisation.

Successful modelling approaches

Different numerical models were presented that were able to accurately reproduce the injection flows measured in the HG-C and HG-D experiments. A modified version of the code TOUGH2 with pressure-dependent permeability was used to simulate the water injection phase of HG-C. For the gas injection phase of the same experiment, a pathway dilation model, also based on TOUGH2, provided satisfying results. A special feature of this model is the time-dependency of the porosity change. This reflects a time-dependent relaxation of the rock with networks of microscopic pathways that are not in equilibrium with pressure. Another model that was developed for the simulation of the gas injection phase of HG-C was the tube-chamber model. The tube-chamber model is a simple representation of a preferential pathway (a tube containing a porous medium) between the injection interval and an air-filled chamber. The air-filled chamber may be a drained part of a borehole or a fracture inside the rock. A tube-chamber model proved to be sufficient for the simulation of the gas injection phase of the HG-D experiment, too. Different models were needed to simulate the water and gas injection phase of the HG-C experiment. This indicates that a universal model for water and gas injection still has to be found.

The study points out that simple modelling approaches are able to reproduce the main aspects of the water and gas injection experiments under study. The simplifications used in the models include single-phase flow, homogeneous distribution of dilating cracks and the omission of a coupled simulation of flow, stress, and strain evolution. The possibility to omit detailed hydro-mechanical coupling is surprising in view of the well-known importance of hydro-mechanical interactions for gas migration at high pressures. Gerard et al. [18], for instance, have stated the need for a strong hydro-mechanical coupling to reproduce the development of preferential pathways in samples of Callovo-Oxfordian argillite. The applied models showed that the mechanical pro-

cesses in the experiments were simple enough to be approximated by time- and pressure-dependent relations for porosity and permeability. This shows that coupled hydro-mechanical modelling is not always mandatory for processes with hydro-mechanical interactions.

Deriving system properties

The fact that two models reproduced the flow measurements of the HG-C experiment shows that there is no unique physical interpretation of the gas injection phase of the HG-C experiment. The applied tube-chamber model postulates that the injected gas finds its way to a remote air-filled space. This space might be a borehole or some part of the rock that could have been drained during the previous GS-experiment. The pathway dilation model suggests another mechanism. In this model, gas injection is caused by a certain rate of porosity increase inside the rock. A possible reason for such a time-dependent porosity increase is a gradual opening of dead-end crack branches that increases the mean porosity in the clay rock.

This clearly shows that the success of a model to reproduce experimental data does not automatically imply physical correctness and improvement of system understanding. Experimental phenomena may as well be matched by models that are physically incorrect. The two models – the pathway dilation model and the tube chamber model – that were able to provide agreeable fits for the gas injection phase of HG-C cannot both be correct at the same time.

Understanding a system by modelling is difficult if more than one model matches the experimental data. Yet, even then it may be possible to unravel the processes if there are common aspects which run through all models like a red line. The commonalities or invariants of the models likely reflect a feature of the system. The pathway dilation model and tube-chamber model 1, which were used to simulate the gas injection phase of the HG-C experiment, share the following features:

1. There was no water flow in any of the two models. Also, gas and liquid phase did not interact. (Tube-chamber model 1 does not contain any water and the pathway dilation model does not consider water flow, water compression, or gas dissolution.) It should be noted that models that included water compression and gas dissolution did not manage to fit the experimental data in this study.

2. A threshold pressure has to be exceeded in order to trigger gas injection.

3. Once triggered, gas flow persisted even if the injection pressure fell below the initial threshold pressure for gas flow. This "softening" of the material against microscopic tensile failure was described in both models by a lowering of threshold pressures. The same mathematical formulation and the same and threshold-related parameter values were used in this respect.

4. In the pressure regime for the assumed process of pathway dilation, the injection flow was approximately proportional to the injection pressure minus the threshold pressure. The pathway dilation model generates this flow behaviour by introducing a pressure-dependent dilation rate whereas tube-chamber model 1 generates it by a Darcy flow to a distant chamber or cavity.

Assuming that these aspects indeed reflect properties of the system, the following two conclusions can be drawn for the gas injection phase of HG-C. Firstly, the system is virtually a single-phase flow system with minor interactions between the liquid and gas phases. For example, gas flow does not need to displace water as would be the case in the classical two-phase flow theory. Secondly, gas flow is dominated by pressure thresholds, which are amenable to quantification. (The general threshold behaviour of the system is also visible in the water injection phase of the HG-C experiment.)

Interpreting thresholds

The HG-C experiment was regarded as the main resource for the investigation of the flow system. The following thresholds were observed here:

- a threshold of 5 MPa above which water injection was facilitated,

- a threshold of 2.35 MPa for initial gas injection,

- a shut-in threshold of 1.1 MPa for the gas injection phase.

Caution is advised with regard to the HG-D experiment because no flow threshold was observed here. This is unusual for clay rock and might indicate an artefact. Although no flow threshold could be detected in the gas injection phase of the HG-D experiment, a sudden pressure response was noticed in interval 1 of borehole BGS1 as the injection pressure reached a value of 2.3 MPa. This pressure corresponds to the threshold pressure for gas injection during the HG-C experiment.

It is interesting to compare the noticed threshold pressures to the threshold pressures that have been observed at the same site in the GP-A and GS experiments[5] [3]:

- In the GS experiment, the threshold for fracture re-opening by water injection was 4 MPa (phase "hydro 2"). This pressure is lower than the re-opening threshold of 5 MPa that was noticed in the water injection phase of HG-C. The higher value may indicate that mechanical healing took place in the time between the two experiments.

- In all experiments, pressures for fracture opening were higher than for fracture closing both for water and gas injection (phases "hydro 3" and "gas 3" of the GS experiment and phase 2 of the HG-C experiment). Possibly, fracture asperities have introduced a frictional resistance against fracture opening or closure.

- There is a remarkable match between the gas injection thresholds of about 2.350 MPa observed at HG-C and HG-D and the fracture opening threshold of 2.350 MPa that has been noticed in phase "gas 3" of the GS experiment during the injection of gas into the drained fracture.

All in all, there seem to be two threshold levels for the fractured rock at the site: One at 2.35 MPa for gas injection and another at about 4 MPa to 5 MPa for water injection. It is interesting to relate these thresholds to the stress state reported for the Opalinus Clay at the Mont Terri Rock Laboratory. In-situ stress measurements of Corkum and Martin [19] have yielded values of 6.5 MPa, 4.0 MPa, and 2.2 MPa for the first, second, and third principal stress axis, respectively (positive numbers for compression). According to Martin & Lanyon [20] the undisturbed bedding normal stress at the site falls between 4.2 MPa and 4.6 MPa.

There is a striking similarity between the re-opening pressures for water injection (4 MPa for GS and 5 MPa for HG-C) and the normal stress on the bedding plane (4.2 MPa to 4.6 MPa). This is a strong indication that the fractures that have been created in GP-A and reactivated later on in GS and HG-C are mainly aligned parallel to bedding. The assumption that fractures were opened by water injection was confirmed in phase "hydro 2" of the GS experiment. In this phase, FIM measurements of borehole 3 (interval 2) showed a sudden dilation event. This rather points towards a fracture

---

[5] Enachescu et al. [3] related these thresholds to the opening or closure of a fracture.

opening process than to an elastic deformation. The very acute response measured in interval 2 of borehole BGS1 also indicates non-elastic deformation.

The observed thresholds for gas injection (2.35 MPa) agree quite well with the estimated minimum principal stress of 2.2 MPa. This suggests the opening of fractures or fissures that are aligned normal to the axis of the minimum principal stress (which does not exclude that the gas phase also employed fractures that were created parallel to bedding).

Although there is no direct evidence for the existence of dilating gas pathways in the experiments, some arguments speak in favour of pathway dilation. The mentioned correlation between the stress state and the injection pressures for gas entry suggests that there is a transition to tensile failure on the pore scale. This non-elastic process would explain the sharp onset of gas entry that was noticed in the HG-C experiment. A localised crack propagation process resulting in a high localisation of pathways would explain why gas injection could only be modelled by ruling out phase interactions in the present study.

Interpreting the characteristics of water flow

There is something curious about the pressures that were needed for water injection. Firstly, one would not expect a fracturing pressure as high as 9.027 MPa (GP-A experiment) in view of the stress normal to bedding (4.2 MPa to 4.6 MPa) and the respective tensile strength (0.5 MPa as reported by Martin and Lanyon [20]). Secondly, it is not obvious why the water did not activate fractures normal to the minimal principal stress axis. The normal stress on these fractures (2.2 MPa plus tensile strength of approx. 1 MPa)[6] is much lower than the normal stress on the bedding planes (4.2 MPa to 4.6 MPa plus tensile strength of 0.5 MPa).

It seems that water finds it more difficult than gas to enter the rock. This is probably not only caused by the higher viscosity of water. A higher viscosity would attenuate the hydraulic propagation of the pressure signal and delay the dilation process. The very sharp pressure response of borehole BGS1 in phase "hydro 2" of the GS experiment,

---

6 A tensile strength of 1 MPa to 1.5 MPa parallel to bedding and of 0.5 MPa normal to bedding was reported by Martin and Lanyon [18].

which was correlated with a dilation event, clearly differs from such an attenuated behaviour. Also, the higher viscosity of water would not be able to raise the threshold pressure for dilation as it was observed.

The fact that the minimum principal stress was not relevant for water injection rather indicates that water was unable to activate fissures that were aligned normal to the axis of minimum principal stress. Possibly, the apertures of these fissures were so small that the thickness of the water films, which were adsorbed to charged clay minerals, became relevant. This might have reduced the effective porosity and impeded the flow of water, which was necessary for fissure creation and opening.

However, after a prolonged period of fracture drainage, it has been possible to inject water at pressures near to the minimum principal stress (phase "hydro 2" of the GS experiment). Eventually, the fissures normal to the minimum principal stress axis were altered by the previous drainage of the rock. The drying process possibly opened these fissures or destroyed the good fit of the fissure walls.

Opening fractures by water injection seems to be less difficult parallel to bedding. Studies of the three-dimensional pore space geometry of Opalinus Clay have shown a preferential orientation of pore paths parallel to the bedding plane with low tortuosity [21, 22]. This should indeed facilitate water flow and thus a pressure-driven dilation of pathways.

The observed difficulty to inject water may depend on the boundary conditions or on the pace of the pressure build-up. Therefore, care has to be taken when transferring the above findings to other circumstances. Future experiments should investigate the possibility to inject water at lower pressures if the pressure is raised more slowly.

Relevance of tensile strength for gas migration

The fact that similar thresholds for gas injection were observed for disturbed rock (HG-C) and undisturbed rock (HG-D) shows that tensile strength was not relevant for gas migration at the experimental site. However, there is some uncertainty whether undisturbed rock has been tested in the HG-D experiment. The relevance of tensile strength for dilation-driven gas migration in clay rock under repository conditions should therefore be confirmed by further experiments.

7   Conclusions

The present modelling study succeeded to reproduce the injection flows of the HG-C and HG-D experiments with high accuracy. A modified version of the code TOUGH2 with pressure-dependent permeability was used to simulate the water injection phase of HG-C. For the gas injection phase of the same experiment, a pathway dilation model, which was also based on TOUGH2, was developed. A special feature of the pathway dilation model is the time-dependency of the porosity change, which reflects a time-dependent relaxation of the rock with networks of microscopic pathways that are not in equilibrium with pressure. Another type of model, which was developed for the simulation of the gas injection phases, is the tube-chamber model. The tube-chamber model is a simple representation of a preferential pathway (the tube) between the injection borehole and a remote air-filled chamber. The chamber may be a drained part of a borehole or a fracture inside the rock.

The fact that two models reproduced the flow measurements of the HG-C experiment shows that there is no unique physical interpretation of the gas injection phase of the HG-C experiment. The applied tube-chamber model postulates that the injected gas finds its way to a remote air-filled space. This space might be a borehole or some part of the rock that could have been drained during the previous GS-experiment. The pathway dilation model suggests another mechanism. In this model, gas injection is caused by a certain rate of porosity increase inside the rock. A possible reason for such a time-dependent porosity increase is a gradual opening of dead-end crack branches that increases the mean porosity in the clay rock.

Both models, the pathway dilation model and the tube-chamber model, are based on strong simplifications like single-phase flow. No hydro-mechanical coupled modelling has been performed although the dilation process was in fact caused by hydro-mechanical interactions. Yet, simplifying modelling approaches do have advantages because they bring out the main aspects of the system and avoid the generation of models with a lot of parameters whose individual relevance is difficult to see. The applied models showed that the mechanical processes in the experiments were simple enough to be approximated by time- and pressure-dependent relations for porosity and permeability. This shows that coupled hydro-mechanical modelling is not always mandatory for processes with hydro-mechanical interactions.

The simulations showed no evidence of phase interactions such as water displacement, water compression or gas dissolution in the gas injection experiments under study. (Models with increased phase interactions were not able to fit the measured data). This indicates that the interface between gas and liquid phase was small during the experiments, which again suggests a high localisation of gas pathways. Initial thresholds for gas injection roughly agreed with the minimum principal stress for disturbed rock. This and the non-linear character of the flow response indicate the presence of dilating pathways. Shut-in thresholds were lower than the initial thresholds for gas injection, indicating hysteretic processes.

The undisturbed rock, which was tested in the HG-D experiment, showed the same threshold for gas injection as the disturbed rock. This suggests that tensile strength was not relevant for gas migration at the experimental site. However, there is some uncertainty whether undisturbed rock has been tested in the HG-D experiment. Therefore, this finding and its transferability to other sites and conditions should be confirmed by further experiments.

In order to inject water into the saturated system, the injection pressure has to be considerably higher than the minimum principal stress. This phenomenon cannot be explained by viscosity effects alone. Water seemed to be unable to activate fissures aligned normal to the axis of minimum principal stress. Possibly, the apertures of such fissures are so small that water adsorption at mineral surfaces becomes significant and advective flow is impeded. Due to the specific pore structure of the clay it is easier to establish a water flow along the bedding planes than across the bedding planes. This may explain why water apparently prefers to open fractures parallel to the bedding planes (at pressures near to the normal stress on these planes). The difficulty to inject water might decrease if injection pressures are raised more slowly, as would be the case in a repository. Although HG-C and HG-D are long-term experiments, pressurisation has been performed quickly. Slow pressurisation could lead to different filter characteristics of the clay with regard to water flow.

The two-phase flow theory in its pure form does not seem to be appropriate to describe the observed experimental phenomena. Especially, the noticed lack of phase interactions conflicts with this theory. In the two-phase flow theory, gas and liquid share the same pore space, which means that water has to be displaced in order to inject gas into a saturated rock. Also, phase interactions are more intense because gas flow is less localised. The concept of intrinsic permeability, which is part of the two-phase flow

theory and which postulates phase-independent filter characteristics of the rock, becomes meaningless if different pore spaces are used for liquid and gas flow.

The two-phase flow theory is widely considered to be applicable if pathway dilation is absent and swelling effects remain negligible. The theory may therefore still be a reasonable starting point for the development of performance assessment models that also cover the effects of pathway dilation. This study shows that this can be done by implementing pressure- and time-dependent relations. However, two-phase flow models and derivatives usually assume homogeneity and scale-independency. It has to be investigated under which circumstances this is tolerable for highly localised flow paths. Also, the geometry and scale-dependency of gas flow paths has to be studied.

Performance assessment codes must have a certain degree of simplicity in order to cope with large spatial scales or long periods of time. The study showed that simplified assumptions, such as single-phase flow, homogeneous distribution of dilating cracks and omission of hydro-mechanical coupled simulations, can be successful in describing experimental phenomena. However, this does not imply that the models are also suitable for predicting gas migration under conditions relevant to deep geological repositories. The physical processes of gas migration have to be understood more thoroughly in order to be sure that the simplified models capture the main aspects of gas migration. Hydro-mechanical modelling might help to understand the detailed mechanisms of pathway dilation and confirm the validity of simplified modelling approaches.

The onset of pathway dilation increases the complexity of gas migration. However, the observed absence of strong phase interactions raises hope to find performance assessment models with manageable complexity in the future.

Yet, predicting gas migration in dilating pathways under repository conditions remains a complicated task. The prospects to find appropriate performance assessment models for this complex process in the future should therefore be balanced against engineering options that keep gas pressures below the threshold for pathway dilation. A pressure reduction could, for instance, be achieved by providing additional pore space for gas storage or by reducing gas production, for example, by waste conditioning, container design or reduced water access to corrodible metals. A pressure limitation would contribute to the simplicity and robustness of both the repository system and the safety assessment.

Acknowledgements

References

[1]   Marschall, P., S. Horseman, and T. Gimmi (2005): Characterisation of Gas
        Transport Properties of the Opalinus Clay, a Potential Host Rock Formation for
        Radioactive Waste Disposal. Oil and Gas Science and Technology, 60(1):
        p. 121-139.

[2]   Navarro, M. (2009): Simulating the migration of repository gases through
        argillaceous rock by implementing the mechanism of pathway dilation into the
        code TOUGH2 (TOUGH2-PD). PAMINA project, public milestone 3.2.14.
        Gesellschaft für Anlagen- und Reaktorsicherheit (GRS) mbH, Cologne.

[3]   Enachescu, C., P. Blümling, A. Castelao, and P. Steffen (2002): Mont Terri GP-
        A and GS Experiments, Synthesis Report. Internal Report 02-51.

[4]   Trick, T. (2007): Mt. Terri HG-C Experiment Phase 1, First hydraulic tests and
        deformation measurements in borehole BGS2 (Mt. Terri Phase 12). Solexperts
        AG, Report TN 2007-13.

[5]   Rösli, U. and T. Trick (2008): Mt. Terri HG-C Experiment Phase 2, Hydraulic
        and gas test series in BGS2 borehole and deformation measurements in BGS3
        and BGS4 boreholes. Report TN 2008-80.

[6]   Organization for Economic Co-operation and Development - Nuclear Energy
        Agency (OECD-NEA) (2001): Gas Generation and Migration in Radioactive
        Waste Disposal. Workshop Proceedings, Reims, France, 26-28 June 2000,
        ISBN 92-64-18672-7, 190 p., Paris.

[7]   Rodwell, W., W. Cool, M. Cunado, L. Johnson, M. Mäntynen, W. Müller, P.
        Sellin, M. Snellman, J. Talandier, T. Vieno, and S. Vines (2003): A thematic
        network on gas issues in safety assessment of deep repositories for radioactive
        waste (Gasnet). European Commission, EUR 20620EN, Final Report, 45 p.

[8]   Alonso, E.E., S. Olivella, and D. Arnedo (2006): Mechanisms of Gas Transport
        in Clay Barriers. Journal of Iberian Geology, 32(2): p. 175-196.

[9]   Olivella, S. and E.E. Alonso (2008): Gas flow through clay barriers.
        Géotechnique, 58(3): p. 157–176.

[10]   Finsterle, S. (2009): iTOUGH2-IFC: An Integrated Flow Code in Support of Nagra's Probabilistic Safety Assessment. User's Guide and Model Description. Lawrence Berkeley National Laboratory, LBNL-1441E, Berkeley, CA (US).

[11]   Yu, L., E. Weetjens, J. Perko, and D. Mallants (2011): Comparison of Numerical Tools Through Thermo-Hydro-Gas Transport Modelling for a Geological Repository in Boom Clay. TOUGH2 Symposium 2009, Berkeley, California , USA, 174(3): p. 411-423.

[12]   Enssle, C.P., J. Croisé, A. Poller, G. Mayer, and J. Wendling (2011): Full scale 3D-modelling of the coupled gasmigration and heat dissipation in a planned repository for radioactive waste in the Callovo-Oxfordian clay. Physics and Chemistry of the Earth – Clays in Natural and Engineered Barriers for Radioactive Waste Confinement, 36(17–18): p. 1754-1769.

[13]   Pruess, K. (1990): TOUGH2: A general purpose numerical simulator for multiphase fluid flow. Lawrence Berkeley National Laboratory, University of California, Report LBL-29400, Berkeley, California, USA.

[14]   Pruess, K. (1991): EOS7: An equation of state module for TOUGH2. Lawrence Berkeley National Laboratory, Report LBL-31114, Berkeley, California, USA.

[15]   Pruess, K.O., C.; Moridis, G. (1999): TOUGH2 User's Guide, Version 2.0. Earth Sciences Division, Lawrence Berkeley National Laboratory, University of California, LBNL-43134, Berkeley, California, USA.

[16]   Rösli, U. (2010): HG-D Experiment (Reactive gas transport in OPA), Hydraulic HI tests in borehole BHG-D1 (interval 2). Solexperts AG, Technical Note 2010-46.

[17]   Bock, H. (2000): RA experiment - Rock mechanics analyses and synthesis: Data report on rock mechanics. Mont Terri Technical Report, TR 2000-02.

[18]   Gerard, P.H., J.; Charlier, R.; Collin, F. (2012): Hydro-Mechanical Coupling of the Development of Preferential Gas Pathways in Claystone. Unsaturated Soils: Research and Applications: p. 175-180.

[19]   Corkum, A.G. and C.D. Martin (2007): Modelling a Mine-by Test at the Mont Terri Rock Laboratory, Switzerland. Int. J. Rock Mech. Min. Sci., 44: p. 846-885.

[20]   Martin, C.D. and G.W. Lanyon (2003): Measurement of in-situ stress in weak rocks at Mont Terri Lock Laboratory, Switzerland. International Journal of Rock Mechanics and Mining Sciences, 40(7-8): p. 1077-1088.

[21]   Keller, L.M.H., L.; Wepf, R.; Gasser, P. (2011): 3D geometry and topology of pore pathways in Opalinus clay: Implications for mass transport. Applied Clay Science, 52(1-2): p. 85–95.

[22]   Keller, L.M.H., L.; Wepf, R.; Gasser, P.; Münch, B.; Marschall, P. (2011): On the application of focused ion beam nanotomography in characterizing the 3D pore space geometry of Opalinus clay. Physics and Chemistry of the Earth, 36(17-18): p. 1539–1544.

List of figures

List of tables